Energy-Efficient Beamforming Design for Integrated Sensing and Communications Systems

Jiaqi Zou, *Graduate Student Member, IEEE*, Songlin Sun, *Senior Member, IEEE*, Christos Masouros, *Fellow, IEEE*, Yuanhao Cui, *Member, IEEE*, Ya-Feng Liu, *Senior Member, IEEE*, and Derrick Wing Kwan Ng, *Fellow, IEEE*

***Abstract*—In this paper, we investigate the design of energy-efficient beamforming for an ISAC system, where the transmitted waveform is optimized for joint multi-user communication and target estimation simultaneously. We aim to maximize the system energy efficiency (EE), taking into account the constraints of a maximum transmit power budget, a minimum required signal-to-interference-plus-noise ratio (SINR) for communication, and a maximum tolerable Cramér-Rao bound (CRB) for target estimation. We first consider communication-centric EE maximization. To handle the non-convex fractional objective function, we propose an iterative quadratic-transform-Dinkelbach method, where Schur complement and semi-definite relaxation (SDR) techniques are leveraged to solve the subproblem in each iteration. For the scenarios where sensing is critical, we propose a novel performance metric for characterizing the sensing-centric EE and optimize the metric adopted in the scenario of sensing a point-like target and an extended target. To handle the nonconvexity, we employ the successive convex approximation (SCA) technique to develop an efficient algorithm for approximating the nonconvex problem as a sequence of convex ones. Furthermore, we adopt a Pareto optimization mechanism to articulate the tradeoff between the communication-centric EE and sensing-centric EE. We formulate the search of the Pareto boundary as a constrained optimization problem and propose a computationally efficient algorithm to handle it. Numerical results validate the effectiveness of our proposed algorithms compared with the baseline schemes and the obtained approximate Pareto boundary shows that there is a non-trivial tradeoff between communication-centric EE and sensing-centric EE, where the number of communication users and EE requirements have serious effects on the achievable tradeoff.**

***Index Terms*—Integrated sensing and communication (ISAC), energy efficiency, fractional programming.**

Part of this work has been accepted by the IEEE Global Communications Conference (GLOBECOM 2023) for publication [1]. *(Corresponding author: Songlin Sun.)*

Jiaqi Zou is with the School of Information and Communication Engineering, Beijing University of Posts and Telecommunications, Beijing 100876, China, and also with the Department of Electrical and Electronic Engineering, University College London, London WC1E 7JE, UK, and also with the Key Laboratory of Trustworthy Distributed Computing and Service (BUPT), Ministry of Education, China, and also with the National Engineering Laboratory for Mobile Network Security, BUPT, Beijing, China (e-mail: jqzou@bupt.edu.cn).

Songlin Sun is with the School of Information and Communication Engineering, Beijing University of Posts and Telecommunications, Beijing 100876, China, and also with the Key Laboratory of Trustworthy Distributed Computing and Service (BUPT), Ministry of Education, China, and also with the National Engineering Laboratory for Mobile Network Security, BUPT, Beijing, China (e-mail: slsun@bupt.edu.cn).

Christos Masouros is with the Department of Electrical and Electronic Engineering, University College London, WC1E 7JE, UK (e-mail: chris.masouros@ieee.org). This work was supported by the project 6GMUSICAL, under the Smart Networks and Services Joint Undertaking (SNS JU) under the European Union's Horizon Europe research and innovation programme under Grant Agreement No. 101139176.

Yuanhao Cui is with the Department of Electronic and Electrical Engineering, Southern University of Science and Technology, Shenzhen 518055, China (e-mail: cuiyh@sustech.edu.cn).

Ya-Feng Liu is with the State Key Laboratory of Scientific and Engineering Computing, Institute of Computational Mathematics and Scientific/Engineering Computing, Academy of Mathematics and Systems Science, Chinese Academy of Sciences, Beijing 100190, China (e-mail: yafliu@lsec.cc.ac.cn). The work of Y.-F. Liu was supported in part by the National Natural Science Foundation of China (NSFC) under Grant 12371314 and Grant 12288201.

Derrick Wing Kwan Ng is with the School of Electrical Engineering and Telecommunications, University of New South Wales, Sydney, NSW 2052, Australia (e-mail: w.k.ng@unsw.edu.au).

I. Introduction

Integrated sensing and communications (ISAC) are anticipated as a viable enabling technology for unlocking the potential of next-generation wireless networks, as the two kinds of systems tend to share various common devices, signal processing techniques, and even the hardware circuitries. Rather than the conventional parallel development of the two systems, the joint designs advocating their coexistence and cooperation have attracted extensive research interest in recent years [2]. For instance, the coexistence of communication and radar systems focuses on spectrum sharing or physical integration design, which mainly aims to mitigate mutual interference and efficiently manage the limited wireless resources [3]–[5]. Indeed, since communication and radar systems may transmit independent signals superimposed in the time/frequency domains, the interference between each other should be minimized to facilitate their individual functionalities. In such cases, numerous approaches have been proposed, such as cooperative spectrum sharing [6] and beamforming design [7]. Nevertheless, the existence of inevitable mutual interference still causes certain limitations on spectral efficiency performance.

Meanwhile, compared with the coexistence design approaches that generate communication and sensing signals separately, ISAC employs a common transmitted signal for realizing communication and sensing simultaneously. In such a case, the crux of ISAC is how to design a specialized waveform for effectively transmitting data and sensing potential targets. In particular, the waveform design can be categorized into the communication-centric, radar-centric, and joint design according to the design goals [8]–[10]. Specifically, the radar-centric design aims to modulate the communication data onto the radar pulses, where the radar probing signals can be regarded as an information carrier [11]. On the other hand,

communication-centric approaches utilize existing communication signals to sense the environment, such as cellular signals [12] and Wi-Fi signals [13]. In particular, various environmental conditions can be extracted from the received echoes of the communication signals, as the target's existence or movement inevitably affects the signal's propagation. Nevertheless, the integration performance is limited in the above two approaches, as the communication/sensing functionality is often carried out as ancillary tasks. In contrast, the joint ISAC design studies the co-design of signaling methodologies enabling both communications and sensing, which is the research content of this work.

A. Related Works

One of the key challenges in joint waveform design is to strike a balance between the tradeoff of communication and sensing. A pioneer work of [14] investigated embedding communication data by manipulating sidelobes within the MIMO radar's spatial beampattern, while reserving the mainlobe for target detection. Although this method paved the way for the development of dual-functional transmitter design, the related beampattern optimization was not studied. This research gap was addressed by [15] that studied the dual-functional beampattern, where the Cramér-Rao bound (CRB) was minimized subject to the constraint of the minimum required signal-to-interference-plus-noise ratio (SINR) at each communication user. Subsequently, the fundamental tradeoff between the CRB for target parameter estimation and the data rate for communication was also investigated in [16], [17] under various system settings, thereby unveiling the potential of ISAC.

Despite the aforementioned approaches can achieve a favorable tradeoff between radar sensing and data transmission [16], [17], the energy efficiency (EE) optimization of the joint waveform has not been fully investigated. Currently, the energy consumption of state-of-the-art fifth-generation (5G) wireless networks is extremely high, resulting in expensive operational costs [18]–[20]. It is anticipated that the upcoming ISAC will consume significant energy than the current ones, as the wireless signals are expected to serve the dual purposes of environment sensing and information transmission simultaneously. This increase in energy consumption may hinder the long-term development of sustainable and environmentally friendly wireless communication technologies. It is also worth noting that existing well-investigated communication-only energy-efficient designs cannot be directly applied to ISAC, e.g., [18]–[20], as they do not take sensing functionalities into consideration. Hence, there is an urgent need to investigate the energy efficiency design of ISAC for establishing perceptive-efficient and spectrally-efficient cellular networks.

Recently, a few works have studied ISAC beamforming for maximizing communication-centric EE. For instance, the work [21] investigated the communication EE maximization under the required radar beampattern constraint. Yet, it does not consider the sensing EE and the performance of target parameter estimation. Besides, the work [22] focused on energy minimization under the sensing and communication constraints. However, the algorithm designed in [22] cannot handle the EE optimization due to the intrinsic challenges brought by fractional programming in the resource allocation design. More importantly, to the best of our knowledge, the sensing-centric EE that characterizes the EE of target sensing has been rarely studied in the literature. In particular, to fulfill the increasing demand for sensing services, it is natural for the base station (BS) to transmit the waveforms with high power for improving the detection and estimation performance. However, this operation will inevitably bring unaffordable energy costs, which contradicts the emerging requirements of carbon neutrality and environmental sustainability for future wireless networks [18]. Therefore, designing an energy-efficient sensing performance metric for ISAC is of utmost importance.

B. Contributions

Against this background, this work considers the EE optimization for the waveform design of ISAC, where the communication-centric EE, sensing-centric EE, and their tradeoffs are investigated. Specifically, for the ISAC systems wherein communication serves as the primary objective, we study the ISAC waveform design for maximizing the communication-centric EE, i.e., the ratio of the achievable rate and the corresponding power consumption, while guaranteeing both the target estimation and communication performance in terms of the CRB and SINR, respectively. As for the sensing-centric ISAC systems, for the first time, we propose the performance metric to measure the sensing-centric EE for target parameter estimation. Then, we optimize the ISAC waveform to maximize the sensing-centric EE, considering the constraints of SINR, CRB, and the maximum transmission power budget. Then, we study the Pareto boundary of communication-centric EE and sensing-centric EE for characterizing their tradeoffs. The main contributions of this paper are summarized as follows.

- We optimize the communication-centric EE considering the two scenarios having a point-like target estimation and an extended target estimation, respectively, under the constraints of CRB, SINR, and transmission power limitations. For the case of point-like target, the nonconvexity of the objective function and CRB constraint hinder the communication-centric EE optimization. For handling these challenges, we first adopt the quadratic-transform-Dinkelbach method to reformulate the nonconvex fractional objective function as a tractable formulation. Then, we adopt the semi-definite relaxation and linear matrix inequality to convert the nonconvex optimization problem into a sequence of convex optimization problems. Finally, we generalize the proposed algorithm to an extended target case.
- We propose a performance metric for capturing the notion of sensing-centric EE for the first time, which adopts the ratio of the reciprocal of the CRB to the transmit energy for measuring "*information-per-Joule*". Then, based on the proposed metric, we consider the sensing-centric EE maximization for point-like/extended targets by optimizing the transmit beamforming. Although the considered

problem is nonconvex, we adopt the Schur complement to reformulate the problem into a tractable formulation, facilitating the development of a successive convex approximation (SCA)-based algorithm to effectively acquire the solution to the design problem.

- We adopt the Pareto optimization technique to characterize the tradeoff between the communication-centric EE and the sensing-centric EE. In particular, we formulate a constrained optimization problem that maximizes the communication-centric EE under the constraint of sensing-centric EE. To handle the nonconvexity of the considered optimization problem, we propose an SCA-based iterative algorithm for addressing the nonconvexity. Then, by varying the threshold of the sensing-centric EE, the approximate Pareto boundary can be obtained by solving a sequence of constrained problems. Simulation results present the Pareto boundary to demonstrate the tradeoff between the two EE metrics.

The remainder of this paper is organized as follows. Section II introduces the system model, including the communication model and the sensing model. In Section III, we study the optimization of the communication-centric EE under the sensing and communication constraints. The sensing-centric EE is studied in Section IV. Section V investigates the tradeoff between the communication-centric and the sensing-centric EE. Simulation results are provided in Section VI. Finally, we conclude the paper in Section VII.

Notations: The normal plain text (i.e., t), bold lowercase letters (i.e., $\mathbf{w}$) and uppercase letters (i.e., $\mathbf{W}$) represent scalars, vectors, and matrices, respectively. $\mathrm{tr}(\cdot)$, $\mathrm{rank}(\cdot)$, $(\cdot)^H$, and $(\cdot)^T$ denote the trace operator, the rank operator, the Hermitian transpose, and the transpose operator, respectively. $\mathbb{C}^{n\times n}$ stands for an $n\times n$ complex-valued matrix. $\|\cdot\|$ represents the L_2 norm of a matrix. The inequality $\mathbf{A}\succeq\mathbf{0}$ means that $\mathbf{A}$ is Hermitian positive semi-definite. $\mathrm{Re}(\cdot)$ denotes the real part of the argument. We adopt $\mathbb{E}(\cdot)$ for the stochastic expectation. $\dot{f}(x)$ denotes the first derivative of function $f(x)$. The notation $\triangleq$ is used for definitions.

II. System Model

As depicted in Fig. 1, we consider an ISAC multiple-input multiple-output (MIMO) system, where the BS equipped with M transmit antennas serves K single-antenna UEs for communication with $K\leq M$. Let $k\in\mathcal{K}\triangleq\{1,2,\cdots,K\}$ denote the communication user set. As for radar estimation, the environmental information is simultaneously extracted from the reflected echoes with N receiving antennas implemented at the BS. To avoid the potential of sensing information loss, similar to [15], we assume that the number of transmit antennas is less than or equal to that of receive antennas, i.e., $M\leq N$. As for target sensing, both the point-like target and the extended target cases are considered separately covering various practical scenarios. In particular, the former case denotes the unstructured point that is far away from the BS, such as unmanned aerial vehicles (UAVs). On the other hand, for the extended target, it acts as a reflecting surface with a large number of distributed scatterers, such as a vehicle or a pedestrian [15]. The detailed model is given as follows.

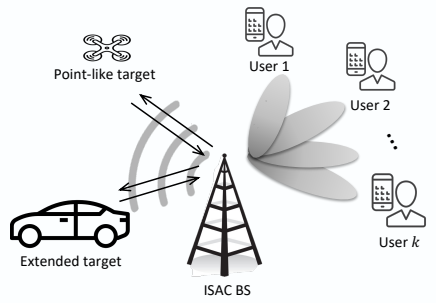

Fig. 1: An illustration of an ISAC MIMO system where an ISAC BS simultaneously serves multiple communication users and senses a point-like target or an extended target.

A. Communication Model

We denote the beamforming vector and the channel from the BS to the k-th user as $\mathbf{w}_k\in\mathbb{C}^{M\times1}$ and $\mathbf{h}_k\in\mathbb{C}^{M\times1}$, respectively. Then, the data symbol intended for the k-th user at time slot l is denoted as $s_k[l]$, with unit power $\mathbb{E}\left(|s_k[l]|^2\right)=1$. Left multiplying $\mathbf{s}[l]=[s_1[l],s_2[l],\cdots,s_k[l]]^T\in\mathbb{C}^{K\times1}$ with the beamforming matrix $\mathbf{W}=[\mathbf{w}_1,\mathbf{w}_2,\cdots,\mathbf{w}_k]\in\mathbb{C}^{M\times K}$, the transmitted signal vector of the BS is given by $\mathbf{x}[l]=\mathbf{W}\mathbf{s}[l]$. Then, the transmitted ISAC waveform over L time slots can be denoted as $\mathbf{X}=[\mathbf{x}[1],\mathbf{x}[2],\cdots,\mathbf{x}[L]]\in\mathbb{C}^{M\times L}$. Then, the received signal at the k-th user during the l-th time slot, $l\in\{1,2,\cdots,L\}$, is given as follows

$$y_k[l]=\mathbf{h}_k^H\mathbf{w}_k s_k[l]+\sum_{j=1,j\neq k}^{K}\mathbf{h}_k^H\mathbf{w}_j s_j[l]+z_c[l], \quad (1)$$

where $z_c[l]$ is the additive white Gaussian noise (AWGN) with zero mean and variance σ_c^2. The received SINR at the k-th user can be calculated as

$$\mathrm{SINR}_k(\mathbf{W})=\frac{\left|\mathbf{h}_k^H\mathbf{w}_k\right|^2}{\sigma_c^2+\sum_{j=1,j\neq k}^{K}\left|\mathbf{h}_k^H\mathbf{w}_j\right|^2}, \quad (2)$$

and the corresponding achievable rate is $R_k(\mathbf{W})=\log_2(1+\mathrm{SINR}_k(\mathbf{W}))$.

It is well known that communication-centric EE is defined as a ratio of the transmission sum rate $\sum_k R_k(\mathbf{W})$ to the total power consumption P. Following [23], [24], the power consumption can be calculated as

$$P=\frac{1}{\epsilon}P_d+P_0, \quad (3)$$

where $P_d=\sum_k\|\mathbf{w}_k\|_2^2$ and $\epsilon\in[0,1]$ denote the total power consumption of the transmitted data and the power amplifier efficiency, respectively. P_0 denotes the sum of the power consumed by the circuitries in the RF chains and the power consumption of the BS including power supply, cooling system, etc. As it is still an open issue to accurately quantify P_0, we follow [25], [26] to assume P_0 as a constant. Note that the impact of values of P_0 on the system performance will be investigated in the simulation section. Hence, the communication-centric EE, measuring the required "bits-per-

Joule" [18], [25], can be calculated as

$$\mathrm{EE_C} = \frac{R_k(\mathbf{W})}{P} = \frac{\sum_k \log_2\left(1+\left|\mathbf{h}_k^H\mathbf{w}_k\right|^2 \Big/ \left(\sigma_c^2+\sum_{j=1,j\neq k}^K \left|\mathbf{h}_k^H\mathbf{w}_j\right|^2\right)\right)}{\frac{1}{\epsilon}\sum_k \|\mathbf{w}_k\|_2^2 + P_0}. \tag{4}$$

B. Sensing Model

For radar sensing, the BS exploits the echo signals collected in L time slots to estimate the target parameter. This work considers the two cases with either a point-like target or an extended target, respectively. As we consider the mono-static colocated MIMO radar, we have identical angle of departure (AOD) and angle of arrival (AOA) of the target. For notational simplicity, we denote $\theta_t = \theta_r = \theta$, following the existing literature [15], [27], [28]. Then, for the point-like target that locates in the far field, the target response matrix can be denoted as

$$\mathbf{A} = \alpha \mathbf{a}_r(\theta)\mathbf{a}_t^H(\theta), \tag{5}$$

where $\mathbf{a}_t(\theta)$ and $\mathbf{a}_r(\theta)$ denote the transmit and receive steering vectors for the transmit signal at angle θ, respectively. Following the existing works on ISAC, e.g., [16], [17], we assume that the BS employs a uniform linear antenna with a half-wavelength spacing between the adjacent antennas. Then, the transmit and receive steering vectors are given by

$$\mathbf{a}_t(\theta) = \left[1, \cdots, e^{-j\pi cos\theta}, e^{-j\pi(M-1)cos\theta}\right]^T, \tag{6}$$

$$\mathbf{a}_r(\theta) = \left[1, \cdots, e^{-j\pi cos\theta}, e^{-j\pi(N-1)cos\theta}\right]^T. \tag{7}$$

For the extended target that locates in the near field, we follow [15] to model it as a reflecting surface with N_s point-like scatters. Then, the target response matrix can be represented as

$$\mathbf{A} = \sum_{i=1}^{N_s} \alpha_i \mathbf{a}_r(\theta_i)\mathbf{a}_t^H(\theta_i), \tag{8}$$

where α_i is the reflection coefficient of the i-th scatterer. [1]

Therefore, the received target echoes $\mathbf{Y}_\mathrm{R}$ from the point-like or the extended targets can both be denoted as

$$\mathbf{Y}_\mathrm{R} = \mathbf{A}\mathbf{X} + \mathbf{Z}_s, \tag{9}$$

where $\mathbf{Z}_s$ is the zero-mean AWGN with variance σ_s^2 in each element.

Since CRB is a lower bound on the variance of an unbiased estimator of an unknown parameter that can guarantee the performance of sensing [15], [17], we adopt the CRB as the sensing metric to design the energy-efficient ISAC in the following.

[1]Note that the extended target reflects $N_s > 1$ scatters, consisting of multiple signal paths with different angles. As the BS has no prior knowledge about the distribution of the scatters and cannot distinguish N_s scatterers lying within the same range bin, the BS is required to estimate $\mathbf{A}$ instead of the angles of all scatters. Then, various algorithms, such as MUSIC [29], can be adopted to calculate the angles of scatters from the estimated $\mathbf{A}$.

III. Communication-Centric Energy-Efficient Design

A. Point-Like Target Case

Since the CRB of α has a similar form as the one of θ, for conciseness, this work only considers the CRB of θ to for the design of the ISAC beamforming. For the point-like target, the CRB of θ is given followed [27], as in (10) at the top of next page, where $\mathbf{R}_\mathbf{x}$ is the sample covariance matrix of $\mathbf{X}$. Since $\mathbb{E}\left(|s_k[l]|^2\right) = 1$, for a large L, we have the asymptotic result $\mathbf{R}_\mathbf{x} = \frac{1}{L}\mathbf{X}\mathbf{X}^H \approx \mathbf{W}\mathbf{W}^H = \sum_{k=1}^K \mathbf{w}_k\mathbf{w}_k^H$ [15].

The communication-centric energy efficient design is to maximize the $\mathrm{EE_C}$ defined in (4), under the constraints of multiple users' required SINR and maximal $\mathrm{CRB}(\theta)$, whose optimization problem can be formulated as follows[2]

$$\max_{\{\mathbf{w}_k\}_{k=1}^K} \frac{\sum_{k=1}^K \log_2\left(1+\left|\mathbf{h}_k^H\mathbf{w}_k\right|^2 \Big/ \left(\sigma_c^2+\sum_{j=1,j\neq k}^K \left|\mathbf{h}_k^H\mathbf{w}_j\right|^2\right)\right)}{\frac{1}{\epsilon}\sum_k \|\mathbf{w}_k\|_2^2 + P_0} \tag{11a}$$

$$\text{s.t.} \quad \sum_{k=1}^K \|\mathbf{w}_k\|_2^2 \le P_{\max}, \tag{11b}$$

$$\mathrm{CRB}(\theta) \le \rho, \tag{11c}$$

$$\frac{\left|\mathbf{h}_k^H\mathbf{w}_k\right|^2}{\sigma_c^2 + \sum_{j=1,j\neq k}^K \left|\mathbf{h}_k^H\mathbf{w}_j\right|^2} \ge \gamma_k, \forall k, \tag{11d}$$

where $P_{\max}$ denotes the power budget of the BS and (11b) is the transmit power constraint. Besides, ρ and γ_k are the required CRB threshold for sensing and the required SINR for the k-th communication user, respectively. In general, it is challenging to solve problem (11) directly, due to the nonconvexity of the fractional objective function (11a) and nonconvex constraints (11c) and (11d).

For addressing the nonconvex optimization problem, we first adopt the Dinkelbach's method [31] to reformulate the problem (11) as

$$\max_{\{\mathbf{w}_k\}_{k=1}^K} \quad f_1(\mathbf{w}_k) - \lambda f_2(\mathbf{w}_k) \tag{12a}$$

$$\text{s.t.} \quad (11b),\ (11c),\ (11d), \tag{12b}$$

where $f_1(\mathbf{w}_k) \triangleq \sum_{k=1}^K \log_2\left(1+\frac{\left|\mathbf{h}_k^H\mathbf{w}_k\right|^2}{\sigma_c^2+\sum_{j=1,j\neq k}^K \left|\mathbf{h}_k^H\mathbf{w}_j\right|^2}\right)$, $f_2(\mathbf{w}_k) \triangleq \frac{1}{\epsilon}\sum_{k=1}^K \|\mathbf{w}_k\|_2^2 + P_0$, and $\lambda \ge 0$ is the auxiliary variable to be iteratively updated by

$$\lambda = \frac{f_1(\mathbf{w}_k)}{f_2(\mathbf{w}_k)}. \tag{13}$$

With (12) and (13), an efficient solution to problem (11) can be obtained by updating $\mathbf{w}_k$ and λ alternately.

[2]For brevity in our presentation, we focus solely on the CRB of angle estimation to illustrate our proposed energy efficiency design. However, it is worth mentioning that the proposed algorithm can be generalized to involve the CRB for the joint estimation of angle and distance. Specifically, since the distance can be estimated from the signal propagation delay [30], the CRB for the joint estimation of angle and time delay can be derived as shown in Appendix A, i.e., $\mathrm{CRB}_{\hat{\theta}}$ in (56) and CRB_{τ} in (57). As $\mathrm{CRB}_{\hat{\theta}}$ and CRB_{τ} share nearly identical formulation as $\mathrm{CRB}(\theta)$ in (10), this generalization is naturally facilitated.

$$\mathrm{CRB}(\theta)=\frac{\sigma_s^2}{|\alpha|^2\left(M\dot{\mathbf{a}}^H(\theta)\mathbf{R}_{\mathbf{x}}^T\dot{\mathbf{a}}(\theta)+\mathbf{a}^H(\theta)\mathbf{R}_{\mathbf{x}}^T\mathbf{a}(\theta)\left\|\dot{\mathbf{a}}(\theta)\right\|^2-\frac{M|\mathbf{a}^H(\theta)\mathbf{R}_{\mathbf{x}}^T\dot{\mathbf{a}}(\theta)|^2}{\mathbf{a}^H(\theta)\mathbf{R}_{\mathbf{x}}^T\mathbf{a}(\theta)}\right)}, \tag{10}$$

Nevertheless, problem (12) is still difficult to handle due to the following issues: 1) the objective function (12a) is still non concave over $\{\mathbf{w}_k\}$ due to the fractional function $f_1(\mathbf{w}_k)$; 2) nonconvex constraints (11c) and (11d). Since the function $\log_2(\cdot)$ is concave and non-decreasing, the nonconvexity of (12a) can be addressed if the term inside $\log_2(\cdot)$ can be reformulated as an equivalent concave formulation. Bearing this in mind, since $f_1(\mathbf{w}_k)$ belongs to the general multiple-ratio concave-convex fractional programming problem, we adopt the quadratic transform method [32, Theorem 1] to reformulate $f_1(\mathbf{w}_k)$ as

$$f_1(\mathbf{w}_k)=\max_{t_k}\sum_{k=1}^{K}\log_2\left(1+2t_k\,\mathrm{Re}(\mathbf{w}_k^H\mathbf{h}_k)-t_k^2B_k(\mathbf{w}_k)\right), \tag{14}$$

where $B_k(\mathbf{w}_k)=\sigma_c^2+\sum_{j=1,j\neq k}^{K}\left|\mathbf{h}_k^H\mathbf{w}_j\right|^2$ and t_k is an introduced auxiliary variable that is iteratively updated by

$$t_k=\left|\mathbf{h}_k^H\mathbf{w}_k\right|\left(\sigma_c^2+\sum_{j=1,j\neq k}^{K}\left|\mathbf{h}_k^H\mathbf{w}_j\right|^2\right)^{-1}. \tag{15}$$

Based on the above reformulations, problem (11) can be recast as

$$\begin{aligned}\max_{\{\mathbf{w}_k,t_k\}_{k=1}^K,\lambda}\quad&\sum_{k=1}^{K}\log_2\left(1+2t_k\,\mathrm{Re}(\mathbf{w}_k^H\mathbf{h}_k)-t_k^2B_k(\mathbf{w}_k)\right)\\&-\lambda\left(\frac{1}{\epsilon}\sum_{k=1}^{K}\|\mathbf{w}_k\|_2^2+P_0\right)\quad\text{s.t.}\quad(12b),\end{aligned} \tag{16}$$

where $\{\mathbf{w}_k,t_k\}_{k=1}^K$ and λ can be updated alternatively.

In the following, we focus on handling the nonconvex constraints (11c) and (11d). Specifically, constraint (11c) can be reformulated as

$$\begin{aligned}&M\dot{\mathbf{a}}^H(\theta)\mathbf{R}_{\mathbf{x}}^T\dot{\mathbf{a}}(\theta)+\mathbf{a}^H(\theta)\mathbf{R}_{\mathbf{x}}^T\mathbf{a}(\theta)\left\|\dot{\mathbf{a}}(\theta)\right\|^2\\&-\frac{M\left|\mathbf{a}^H(\theta)\mathbf{R}_{\mathbf{x}}^T\dot{\mathbf{a}}(\theta)\right|^2}{\mathbf{a}^H(\theta)\mathbf{R}_{\mathbf{x}}^T\mathbf{a}(\theta)}-\frac{\sigma_s^2}{2L\rho\left|\alpha\right|^2}\geq 0.\end{aligned} \tag{17}$$

Then, for notational conciseness, denoting $\mathcal{F}(\mathbf{R}_{\mathbf{X}})\triangleq M\dot{\mathbf{a}}^H(\theta)\mathbf{R}_{\mathbf{x}}^T\dot{\mathbf{a}}(\theta)+\mathbf{a}^H(\theta)\mathbf{R}_{\mathbf{x}}^T\mathbf{a}(\theta)\left\|\dot{\mathbf{a}}(\theta)\right\|^2$, (17) can be reformulated as the following linear matrix inequality by leveraging the Schur complement [33].

$$\begin{bmatrix}\mathcal{F}(\mathbf{R}_{\mathbf{x}})-\frac{\sigma_s^2}{2L\rho|\alpha|^2} & \sqrt{M}\mathbf{a}^H(\theta)\mathbf{R}_{\mathbf{x}}^T\dot{\mathbf{a}}(\theta)\\ \sqrt{M}\dot{\mathbf{a}}^H(\theta)\mathbf{R}_{\mathbf{x}}^T\mathbf{a}(\theta) & \mathbf{a}^H(\theta)\mathbf{R}_{\mathbf{x}}^T\mathbf{a}(\theta)\end{bmatrix}\succeq\mathbf{0}. \tag{18}$$

Next, for handling the nonconvex constraint (11d), we introduce an auxiliary optimization variable matrix $\mathbf{W}_k$ and reformulate constraint (11d) into

$$\mathrm{tr}(\mathbf{Q}_k\mathbf{W}_k)-\gamma_k\sum_{\substack{k\in\mathcal{K}\\j\neq k}}\mathrm{tr}(\mathbf{Q}_k\mathbf{W}_j)\geq\gamma_k\sigma_c^2, \tag{19a}$$

$$\mathbf{W}_k=\mathbf{w}_k\mathbf{w}_k^H, \tag{19b}$$

where $\mathbf{Q}_k=\mathbf{h}_k\mathbf{h}_k^H$. Then, problem (11) can be equivalently reformulated as

$$\begin{aligned}\max_{\{\mathbf{w}_k,\mathbf{W}_k,t_k\}_{k=1}^K}\quad&\sum_{k=1}^{K}\log_2\left(1+2t_k\,\mathrm{Re}(\mathbf{w}_k^H\mathbf{h}_k)-t_k^2B_k(\mathbf{W}_k)\right)\\&-\lambda\left(\frac{1}{\epsilon}\sum_{k=1}^{K}\mathrm{tr}(\mathbf{W}_k)+P_0\right)\end{aligned} \tag{20a}$$

$$\text{s.t.}\quad\begin{bmatrix}\mathcal{F}(\sum_{k=1}^{K}\mathbf{W}_k)-\frac{\sigma_s^2}{2L\rho|\alpha|^2} & \sqrt{M}\mathbf{a}^H(\theta)\sum\limits_{k=1}^{K}\mathbf{W}_k^T\dot{\mathbf{a}}(\theta)\\ \sqrt{M}\dot{\mathbf{a}}^H(\theta)\sum\limits_{k=1}^{K}\mathbf{W}_k^T\mathbf{a}(\theta) & \mathbf{a}^H(\theta)\sum\limits_{k=1}^{K}\mathbf{W}_k^T\mathbf{a}(\theta)\end{bmatrix}\succeq\mathbf{0}, \tag{20b}$$

$$(11b),\ (19a),\ (19b), \tag{20c}$$

where $B_k(\mathbf{W}_k)\triangleq\sum_{\substack{k\in\mathcal{K}\\j\neq k}}\mathrm{tr}(\mathbf{Q}_k\mathbf{W}_j)+\sigma_c^2$. However, constraint (19b) is a nonconvex equality constraint which is difficult to handle. Therefore, we introduce the following lemma to transform constraint (19b) into equivalent inequality constraints.

Lemma 1: $\mathbf{W}_k=\mathbf{w}_k\mathbf{w}_k^H$ can be equivalently reformulated as

$$\begin{bmatrix}\mathbf{W}_k & \mathbf{w}_k\\ \mathbf{w}_k^H & 1\end{bmatrix}\succeq\mathbf{0},\mathbf{W}_k\succeq\mathbf{0},\forall k, \tag{21a}$$

$$\mathrm{tr}(\mathbf{W}_k)-\mathbf{w}_k^H\mathbf{w}_k\leq 0,\forall k. \tag{21b}$$

Proof: The proof is given in Appendix B. ■

Although the equality constraint in (19b) has been reformulated as the equivalent inequality constraints, constraint (21b) is still nonconvex. For handling this, we adopt the SCA technique that establishes an inner convex approximation of constraint (21b) given as

$$\mathrm{tr}(\mathbf{W}_k)+\left(\mathbf{w}_k^{(i-1)}\right)^H\mathbf{w}_k^{(i-1)}-2\,\mathrm{Re}\left(\left(\mathbf{w}_k^{(i-1)}\right)^H\mathbf{w}_k\right)\leq 0,\forall k, \tag{22}$$

where $\mathbf{w}_k^{(i-1)}$ is the solution obtained at the i-th iteration of the SCA.

Therefore, at the i-th iteration, the convex approximation of

problem (11) can be reformulated as

$$\max_{\mathcal{W},t_k,\lambda} \quad \sum_{k=1}^{K} \log_2\left(1+2t_k\,\mathrm{Re}(\mathbf{w}_k^H\mathbf{h}_k)-t_k^2 B_k(\mathbf{W}_k)\right) - \lambda\left(\frac{1}{\epsilon}\sum_{k=1}^{K}\mathrm{tr}(\mathbf{W}_k)+P_0\right) \tag{23a}$$

$$\text{s.t.} \quad (11b),(19a),(20b),(21a),(22). \tag{23b}$$

Algorithm 1 summarizes the iterative algorithm for handling problem (11), where $\hat{f}_1(\mathbf{w}_k,\mathbf{W}_k) = \sum_{k=1}^{K}\log_2\left(1+2t_k\,\mathrm{Re}(\mathbf{w}_k^H\mathbf{h}_k)-t_k^2B_k(\mathbf{W}_k)\right)$ and $\hat{f}_2(\mathbf{W}_k) = \frac{1}{\epsilon}\sum_{k=1}^{K}\mathrm{tr}(\mathbf{W}_k)+P_0$. Although we cannot guarantee that the optimal solution of problem (11) can be obtained, the proposed Algorithm 1 follows the inexact Dinkelbach-type algorithm adopted in [34], whose convergence can be guaranteed by the following lemma.

Lemma 2: Let $\{\mathbf{w}_k^i,\mathbf{W}_k^i\}$ be the solution sequence generated by solving problem (23). The sequence $\{\lambda^{(i)}\}$ generated by Algorithm 1 is non-decreasing and convergent.

Proof: Since $\hat{f}_1(\mathbf{w}^{(i)},\mathbf{W}^{(i)}) - \lambda^{(i)}\hat{f}_2(\mathbf{W}^{(i)}) = \left(\lambda^{(i+1)}-\lambda^{(i)}\right)\hat{f}_2(\mathbf{W}^{(i)})$, we have $\lambda^{(i+1)} \geq \lambda^{(i)}$ if $\hat{f}_1(\mathbf{w}^{(i)},\mathbf{W}^{(i)}) - \lambda^{(i)}\hat{f}_2(\mathbf{W}^{(i)}) \geq 0$. Obviously, $\hat{f}_1(\mathbf{w}^{(i-1)},\mathbf{W}^{(i-1)}) - \lambda^{(i)}\hat{f}_2(\mathbf{W}^{(i-1)}) = 0$. At the i-th iteration, we approximate problem (11) as problem (23) around $\mathbf{w}_k^{(i-1)}$. Since $\mathbf{w}_k^{(i-1)}$ is definitely a feasible solution of problem (23), we have $\hat{f}_1(\mathbf{w}^{(i)},\mathbf{W}^{(i)}) - \lambda^{(i)}\hat{f}_2(\mathbf{W}^{(i)}) \geq \hat{f}_1(\mathbf{w}^{(i-1)},\mathbf{W}^{(i-1)}) - \lambda^{(i)}\hat{f}_2(\mathbf{W}^{(i-1)}) = 0$. Therefore, we can conclude that the sequence $\{\lambda^{(i)}\}$ is non-decreasing and Algorithm 1 converges due to the finite power budget. ■

Remark 1: Our proposed Algorithm 1 employs Dinkelbach's extended algorithm [35], which is adapted for nonconvex subproblems encountered during iterations. In fact, Dinkelbach's extended algorithm has been widely adopted for handling resource allocation problems in wireless communications, e.g., [36], [37]. As shown in [36], since the solution of each subproblem can be obtained by applying SCA and the sequence generated during iterations is non-decreasing, Algorithm 1 is guaranteed to converge to an efficient solution of problem (11) [35, Theorem 2.2].

Algorithm 1 *: Proposed Iterative Algorithm for Handling Problem* (11)

Set $i=0$, $\delta>0$,$\{\mathbf{w}_k^{(0)},\mathbf{W}_k^{(0)}\}\in\mathcal{S}$;
Initialize $t_k^{(0)},\lambda^{(0)}$ satisfying $\hat{f}_1(\mathbf{w}^{(0)},\mathbf{W}^{(0)}) - \lambda^{(0)}\hat{f}_2(\mathbf{W}^{(0)})\geq 0$;
repeat
  $i\leftarrow i+1$;
  $\tilde{\mathbf{w}}_k^{(i)}\leftarrow\mathbf{w}_k^{(i-1)}$;
  $t_k^{(i)}\leftarrow\frac{\mathrm{Re}(\mathbf{w}_k^{(i-1)^H}\mathbf{h}_k)}{B_k(\mathbf{W}_k^{(i-1)})}$;
  $\lambda^{(i)}\leftarrow\frac{\hat{f}_1(\mathbf{w}_k^{(i-1)},\mathbf{W}_k^{(i-1)})}{\hat{f}_2(\mathbf{W}_k^{(i-1)})}$;
  Solve problem (23a) to obtain the optimal $\mathbf{w}_k^{(i)},\mathbf{W}_k^{(i)}$;
until $\hat{f}_1(\mathbf{w}^{(i)},\mathbf{W}^{(i)}) - \lambda^{(i)}\hat{f}_2(\mathbf{W}^{(i)})$ is less than δ.

Complexity Analysis: The computational complexity of Algorithm 1 is dominated by solving problem (23a). Problem (23a) involves linear matrix inequality (LMI) constraints that dominate the computation complexity. We notice that the problem contains one LMI constraint of size $2M$, K LMI constraints of size $M+1$, and K LMI constraints of size M. Given the required accuracy $\epsilon_0>0$, the ϵ_0-optimal solution can be achieved after a sequence of iterations. Then, the computational complexity can be given as $\mathcal{O}(\sqrt{(2M+1)(K+1)}M^6K^3\ I_{\mathrm{iter}}\ln(1/\epsilon_0))$ by reserving the highest order term, where I_{iter} denotes the number of iterations [38].

Remark 2: Due to the stringent requirement introduced by (22), it is generally non-trivial to directly obtain a feasible solution as an initial point. Alternatively, we can adopt the penalty SCA [39] and introduce auxiliary variables $\bar{\rho}_k$ to transform problem (23) into

$$\max_{\mathcal{W},t_k,\lambda} \quad \sum_{k=1}^{K} \log_2\left(1+2t_k\,\mathrm{Re}(\mathbf{w}_k^H\mathbf{h}_k)-t_k^2 B_k(\mathbf{W}_k)\right) - \lambda\left(\frac{1}{\epsilon}\sum_{k=1}^{K}\mathrm{tr}(\mathbf{W}_k)+P_0\right) - \bar{p}\sum_{k=1}^{K}\bar{\rho}_k \tag{24a}$$

$$\text{s.t.} \quad \mathbf{w}_k^{(i-1)} - 2\,\mathrm{Re}\left(\left(\mathbf{w}_k^{(i-1)}\right)^H\mathbf{w}_k\right)\leq\bar{\rho}_k,\forall k, \tag{24b}$$

$$(11b),(19a),(20b),(21a), \tag{24c}$$

where $\bar{p}$ and $\sum_{k=1}^{K}\bar{\rho}_k$ denote the weight coefficient and the penalty term, respectively. To obtain the initial point of (23), we can solve problem (24) as an initial warm-up phase by gradually raising $\bar{p}$ to induce a reduction in the penalty term to a smaller value. When the penalty term decreases to zero, problem (24) reduces to problem (23), whose solution serves as the feasible initial point of (23).

B. Extended Target Case

For estimating the extended target, we follow [15] to consider the CRB of the target response matrix $\mathbf{A}$ instead of the angle. Since $K\leq M$, transmitting K signal streams is not always sufficient for recovering the rank-M matrix. To address this issue, the BS generates additional signals that are dedicated for target probing. As such, the augmented data matrix at the l-th time slot is $\tilde{\mathbf{x}}[l]\triangleq\left[\mathbf{W},\tilde{\mathbf{W}}\right][\mathbf{s}[l];\tilde{\mathbf{s}}[l]]$, where $\tilde{\mathbf{s}}[l]\in\mathbb{C}^{(N_t-K)\times 1}$ is the dedicated probing signal and $\mathbb{E}\left(\mathbf{s}[l]\tilde{\mathbf{s}}^H[l]\right)=\mathbf{0}$. Note that in the augmented signal, the beamforming $\mathbf{W}=[\mathbf{w}_1,\mathbf{w}_2,\cdots,\mathbf{w}_K]\in\mathbb{C}^{M\times K}$ broadcasts the information data to the K users and the beamforming $\tilde{\mathbf{W}}=[\mathbf{w}_{K+1},\cdots,\mathbf{w}_{K+M}]\in\mathbb{C}^{M\times M}$ is employed to generate probing signals for enabling the estimation of the target response matrix. However, the introduced probing signals $\tilde{\mathbf{s}}[l]$ inevitably generate undesired interference to the served multiple users that introduces non-trivial tradeoff between sensing and communication. In particular, the SINR received at the k-th user is given by

$$\tilde{\mathrm{SINR}}_k=\frac{\left|\mathbf{h}_k^H\mathbf{w}_k\right|^2}{\sum_{i=1,i\neq k}^{K}\left|\mathbf{h}_k^H\mathbf{w}_i\right|^2+\left\|\mathbf{h}_k^H\tilde{\mathbf{W}}\right\|_2^2+\sigma_C^2}, \tag{25}$$

where $\left\|\mathbf{h}_k^H\tilde{\mathbf{W}}\right\|_2^2$ is the additional interference due to the probing signals. In such a case, the CRB for the extended target estimation can be derived as

$$\text{CRB}_{\text{extended}} = \frac{\sigma_s^2 M}{N}\,\text{tr}\left(\mathbf{R}_{\mathbf{x}}{}^{-1}\right), \tag{26}$$

where $\mathbf{R}_{\mathbf{X}} = \mathbf{W}\mathbf{W}^H + \tilde{\mathbf{W}}\tilde{\mathbf{W}}^H$.

Based on the discussions above, the problem of communication-centric EE optimization for estimating an extended target can be formulated as

$$\max_{\{\mathbf{w}_k\}_{k=1}^{K+M}} \quad \frac{\sum_{k=1}^{K}\log_2(1+\tilde{\text{SINR}}_k)}{\frac{1}{\epsilon}\sum_{k=1}^{K+M}\|\mathbf{w}_k\|_2^2 + P_0} \tag{27a}$$

$$\text{s.t.} \quad \sum_{k=1}^{K+M}\|\mathbf{w}_k\|_2^2 \le P_{\max}, \tag{27b}$$

$$\text{CRB}_{\text{extended}} = \frac{\sigma_s^2 M}{L}\,\text{tr}\left(\mathbf{R}_{\mathbf{x}}{}^{-1}\right) \le \tau, \tag{27c}$$

$$\tilde{\text{SINR}}_k \ge \gamma_k. \tag{27d}$$

Obviously, although constraints (27b) and (27c) are both convex, the fractional objective function (27a) is still nonconvex. Following Section III-A, we first adopt Dinkelbach's transformation to handle the nonconvex fractional programming and reformulate the problem as follows

$$\max_{\{\mathbf{w}_k\}_{k=1}^{K+M}} \quad \sum_{k=1}^{K}\log_2(1+\tilde{\text{SINR}}_k) - \lambda\left(\frac{1}{\epsilon}\sum_{k=1}^{K+M}\|\mathbf{w}_k\|_2^2 + P_0\right) \tag{28a}$$

$$s.t. \quad \text{(27b)}, \text{(27c)}, \text{(27d)}. \tag{28b}$$

Then, by exploiting the equality $-\log a = \max_b(\log b - ab)$ [40], problem (28) can be reformulated as problem (29) as shown at the top of the next page. For obtaining a tractable formulation, by introducing auxiliary variables $\mathbf{W}_k \triangleq \mathbf{w}_k\mathbf{w}_k^H, k \in [1,2,\cdots,K]$ and $\mathbf{R}_{\tilde{\mathbf{W}}} = \tilde{\mathbf{W}}\tilde{\mathbf{W}}^H$, problem (29) can be reformulated as problem (30) as shown at the top of the next page.

After inspecting problem (30), we can find that all constraints are convex, except for constraint (30f). Besides, the objective function in (30a) includes three sets of optimization variables: $\{\lambda\}$, $\{b_k\}$, and $\left\{\{\mathbf{W}_k\}_{k=1}^K, \mathbf{R}_{\tilde{\mathbf{W}}}\right\}$. Moreover, when fixing the other two sets, the objective function is convex with respect to the remaining one. Therefore, we first adopt the rank relaxation to remove constraint (30f) and then employ an alternating optimization (AO) algorithm to optimize three sets of optimization variables alternately. The detailed algorithm is summarized in Algorithm 2, where we denote $\tilde{f}_1(\mathbf{W}_k, \mathbf{R}_{\tilde{\mathbf{W}}})$ and $\tilde{f}_2(\mathbf{W}_k, \mathbf{R}_{\tilde{\mathbf{W}}})$ shown in (31) at the top of the next page for brevity.

In the following theorem, we will show that the rank-1 solution of problem (30) can be recovered from the solution generated by Algorithm 2.

Theorem 1: Given the optimal solution obtained by Algorithm 2 as $\{\mathbf{W}_k^*, \mathbf{R}_{\tilde{\mathbf{W}}}^*\}$. When $K = 1$,

$$\hat{\mathbf{W}}^* = \frac{\mathbf{W}^*\mathbf{h}_k\mathbf{h}_k^H\mathbf{W}^*}{\mathbf{h}_k^H\mathbf{W}^*\mathbf{h}_k}, \quad \hat{\mathbf{R}}_{\tilde{\mathbf{W}}}^* = \mathbf{R}_{\tilde{\mathbf{W}}}^* \tag{32}$$

is the optimal rank-1 solution that achieves identical performance as $\{\mathbf{W}_k^*, \mathbf{R}_{\tilde{\mathbf{W}}}^*\}$. When $K > 1$, one can always construct the optimal solution that satisfies the rank-1 constraint acquiring the same performance.

Proof: The proof is given in Appendix C. ■

Complexity Analysis: We provide the computational complexity of Algorithm 2 as follows. Similarly, the problem (30) is a semidefinite program that can be solved by the standard interior-point algorithm. We note that the problem involves $K+1$ LMI constraints of size M. We consider the highest order term and express the computational complexity as $\mathcal{O}(\sqrt{MK+M+K+1}M^6K^3I_{\text{iter}}\log(1/\epsilon_0))$ for an ϵ_0-optimal solution, where I_{iter} represents the number of iterations [38].

Algorithm 2 *: Proposed Iterative Algorithm for Handling* (27)

Set $i = 0$, $\delta > 0$,$\{\mathbf{W}_k^{(0)}, \mathbf{R}_{\tilde{\mathbf{W}}}^{(0)}\} \in \mathcal{S}$, and initialize $\left(b_k^{(0)}, \lambda^{(0)}\right)$ satisfying $\tilde{f}_1(\mathbf{W}_k^{(0)}, \mathbf{R}_{\tilde{\mathbf{W}}}^{(0)}) - \lambda^{(0)}\tilde{f}_2(\mathbf{W}_k^{(0)}, \mathbf{R}_{\tilde{\mathbf{W}}}^{(0)}) \ge 0$;
repeat
$i \leftarrow i+1$;
$\tilde{\mathbf{W}}_k^{(i)}, \mathbf{R}_{\tilde{\mathbf{W}}}^{(i)} \leftarrow \mathbf{W}_k^{(i-1)}, \mathbf{R}_{\tilde{\mathbf{W}}}^{(i-1)}$;
$b_k^{(i)} \leftarrow b_k^{(i-1)}$;
$\lambda^{(i)} \leftarrow \frac{\tilde{f}_1(\mathbf{W}_k^{(i-1)}, \mathbf{R}_{\tilde{\mathbf{W}}}^{(i-1)})}{\tilde{f}_2(\mathbf{W}_k^{(i-1)}, \mathbf{R}_{\tilde{\mathbf{W}}}^{(i-1)})}$;
Solve the rank relaxation of problem (30) to obtain the optimal $\mathbf{W}_k^{(i)}, \mathbf{R}_{\tilde{\mathbf{W}}}^{(i)}, b_k^{(i)}$;
until $\tilde{f}_1(\mathbf{W}_k^{(i)}, \mathbf{R}_{\tilde{\mathbf{W}}}^{(i)}) - \lambda^{(i)}\tilde{f}_2(\mathbf{W}_k^{(i)}, \mathbf{R}_{\tilde{\mathbf{W}}}^{(i)})$ is less than δ.

IV. Sensing-Centric Energy-Efficient Design

A. Performance Metric for Sensing-Centric EE

Recall that in communication-centric designs, EE is generally defined as the ratio of the achievable rate and the power consumption which can measure the amount of communication information per Joule. For sensing, it is well known that Fisher information is the statistical expected value of the observed information about an observable random variable, revealing the highest accuracy (the lowest variance) that can be achieved. It is also well established that CRB is the inverse of Fisher information for unbiased estimators [41], [42]. Considering these, we adopt the reciprocal ratio of the CRB to the transmit power, further normalized by the total time slot length. In this context, we arrive at a novel sensing-centric EE metric defined as

$$\text{EE}_{\text{s}} \triangleq \frac{\text{CRB}^{-1}}{L\left(\frac{1}{\epsilon}\sum_{k=1}^{K}\|\mathbf{w}_k\|_2^2 + P_0\right)}. \tag{33}$$

Both the sensing-centric EE and communication-centric EE measure the "information" per Joule, but the "information" has different meanings. In particular, the sensing-centric EE

$$\max_{\{\mathbf{w}_k\}_{k=1}^{K+M},\{b_k\}_{k=1}^{K},\lambda} \quad \sum_{k=1}^{K}\log_2\left(\left|\mathbf{h}_k^H\mathbf{w}_k\right|^2+\sum_{i=1,i\neq k}^{K}\left|\mathbf{h}_k^H\mathbf{w}_i\right|^2+\left\|\mathbf{h}_k^H\tilde{\mathbf{W}}\right\|_2^2+\sigma_C^2\right) \tag{29a}$$

$$+\sum_{k=1}^{K}\left(\log_2 b_k-b_k(\sum_{i=1,i\neq k}^{K}\left|\mathbf{h}_k^H\mathbf{w}_i\right|^2+\left\|\mathbf{h}_k^H\tilde{\mathbf{W}}\right\|_2^2+\sigma_C^2)\right)-\lambda\left(\frac{1}{\epsilon}\sum_{k=1}^{K+M}\|\mathbf{w}_k\|_2^2+P_0\right)$$

$$\text{s.t.} \quad \text{(27b), (27c), (27d).} \tag{29b}$$

$$\max_{\{\mathbf{W}_k,b_k\}_{k=1}^{K},\mathbf{R}_{\mathbf{W}2},\lambda} \quad \sum_{k=1}^{K}\log_2\left(\mathbf{h}_k^H\left(\mathbf{W}_k+\sum_{i=1,i\neq k}^{K}\mathbf{W}_i+\mathbf{R}_{\tilde{\mathbf{W}}}+\sigma_C^2\right)\mathbf{h}_k\right)$$

$$+\sum_{k=1}^{K}\left(\log_2 b_k-b_k\left(\sum_{i=1,i\neq k}^{K}\mathbf{h}_k^H\mathbf{W}_i\mathbf{h}_k+\mathbf{h}_k^H\mathbf{R}_{\tilde{\mathbf{W}}}\mathbf{h}_k+\sigma_C^2\right)\right)-\lambda\left(\frac{1}{\epsilon}\text{tr}\left(\sum_{k=1}^{K}\mathbf{W}_k+\mathbf{R}_{\tilde{\mathbf{W}}}\right)+P_0\right), \tag{30a}$$

$$\text{s.t. } \text{tr}\left(\sum_{k=1}^{K}\mathbf{W}_k+\mathbf{R}_{\tilde{\mathbf{W}}}\right)\leq P_{\max}, \tag{30b}$$

$$\frac{\sigma_s^2 M}{N}\text{tr}\left(\left(\sum_{k=1}^{K}\mathbf{W}_k+\mathbf{R}_{\tilde{\mathbf{W}}}\right)^{-1}\right)\leq\tau, \tag{30c}$$

$$\mathbf{h}_k\mathbf{W}_k\mathbf{h}_k^H-\gamma_k\left(\sum_{i=1,i\neq k}^{K}\mathbf{h}_k^H\mathbf{W}_i\mathbf{h}_k+\mathbf{h}_k^H\mathbf{R}_{\tilde{\mathbf{W}}}\mathbf{h}_k\right)\geq\gamma_k\sigma_c^2, \tag{30d}$$

$$\mathbf{W}_k\succeq\mathbf{0},\forall k,\mathbf{R}_{\tilde{\mathbf{W}}}\succeq\mathbf{0}, \tag{30e}$$

$$\text{rank}(\mathbf{W}_k)=1,\forall k. \tag{30f}$$

$$\tilde{f}_1(\mathbf{W}_k,\mathbf{R}_{\tilde{\mathbf{W}}})=\sum_{k=1}^{K}\log_2\left(\mathbf{h}_k^H\left(\mathbf{W}_k+\sum_{i=1,i\neq k}^{K}\mathbf{W}_i+\mathbf{R}_{\tilde{\mathbf{W}}}+\sigma_C^2\right)\mathbf{h}_k\right)+\sum_{k=1}^{K}\left(\log_2 b_k-b_k\left(\sum_{i=1,i\neq k}^{K}\mathbf{h}_k^H\mathbf{W}_i\mathbf{h}_k+\mathbf{h}_k^H\mathbf{R}_{\tilde{\mathbf{W}}}\mathbf{h}_k+\sigma_C^2\right)\right) \tag{31a}$$

$$\tilde{f}_2(\mathbf{W}_k,\mathbf{R}_{\tilde{\mathbf{W}}})=\frac{1}{\epsilon}\text{tr}\left(\sum_{k=1}^{K}\mathbf{W}_k+\mathbf{R}_{\tilde{\mathbf{W}}}\right)+P_0. \tag{31b}$$

---

measures the average Fisher information per Joule, i.e., the amount of information that can be extracted by an ideal observer per Joule, with the specific unit also depending on the to-be-estimated parameter. In the following sections, we investigate the sensing-centric EE in cases of estimating a point-like target and an extended target.

Based on the above metric, we study the waveform design to maximize the sensing-centric EE considering the point-like target and the extended target in Sections IV-B and IV-C, respectively.

B. Point-Like Target Case

Considering the point-like target, with the CRB of estimating θ given in (10), the sensing-centric EE optimization problem can be formulated as

$$\max_{\{\mathbf{w}_k\}_{k=1}^{K}} \quad \frac{\text{CRB}^{-1}(\theta)}{L\left(\frac{1}{\epsilon}\sum_{k=1}^{K}\|\mathbf{w}_k\|_2^2+P_0\right)} \tag{34a}$$

$$\text{s.t.} \quad \sum_{k=1}^{K}\|\mathbf{w}_k\|_2^2\leq P_{\max}, \tag{34b}$$

$$\text{CRB}(\theta)\leq\rho, \tag{34c}$$

$$\frac{\left|\mathbf{h}_k^H\mathbf{w}_k\right|^2}{\sigma_c^2+\sum_{j=1,j\neq k}^{K}\left|\mathbf{h}_k^H\mathbf{w}_j\right|^2}\geq\gamma_k,\forall k. \tag{34d}$$

Obviously, problem (34) is also intractable due to the fractional objective function (34a) and nonconvex constraints (34c) and (34d). For handling the fractional objective function (34a), with the introduced auxiliary optimization variables

ω, t, ϕ, and ζ, problem (34) can be reformulated as

$$\max_{\{\mathbf{w}_k\}_{k=1}^K, \omega, \phi, \zeta} \quad \omega \tag{35a}$$

$$\text{s.t.} \quad \text{CRB}(\theta) \leq \frac{1}{t}, \tag{35b}$$

$$\frac{1}{\epsilon}\sum_{k=1}^{K}\|\mathbf{w}_k\|_2^2 + P_0 \leq \phi, t \geq \zeta^2, \tag{35c}$$

$$\omega \leq \frac{\zeta^2}{\phi}, \tag{35d}$$

$$(34b), (34c), (34d).$$

The equivalence between (35) and (34) is obvious, since constraints (35a), (35b), and (35c) should be active at the optimal solution. We note that (35b) share the same form with (11c). Therefore, with the Schur's complement, constraint (35b) can be equivalently reformulated as

$$\begin{bmatrix} \mathcal{F}(\sum_{k=1}^K \mathbf{W}_k) - \frac{t\sigma_s^2}{2L|\alpha|^2} & \sqrt{M}\mathbf{a}^H(\theta)\sum_{k=1}^K \mathbf{W}_k^T \dot{\mathbf{a}}(\theta) \\ \sqrt{M}\dot{\mathbf{a}}^H(\theta)\mathbf{R}_{\mathbf{x}}^T\mathbf{a}(\theta) & \mathbf{a}^H(\theta)\mathbf{R}_{\mathbf{x}}^T\mathbf{a}(\theta) \end{bmatrix} \succeq \mathbf{0}, \tag{36}$$

where $\mathcal{F}(\sum_{k=1}^K \mathbf{W}_k) \triangleq M\dot{\mathbf{a}}^H(\theta)\sum_{k=1}^K \mathbf{W}_k^T\dot{\mathbf{a}}(\theta) + \mathbf{a}^H(\theta)\sum_{k=1}^K \mathbf{W}_k^T\mathbf{a}(\theta)\|\dot{\mathbf{a}}(\theta)\|^2$ and $\mathbf{W}_k = \mathbf{w}_k\mathbf{w}_k^H$. Furthermore, Lemma 1 presents an equivalent formulation of the equality $\mathbf{W}_k = \mathbf{w}_k\mathbf{w}_k^H$ whose convex approximation has been given in (21a) and (22). Then, for handling the fractional constraint (34d), we introduce auxiliary variables $\{\tau_k, \psi_k, \forall k\}$ to reformulate (34d) as

$$\tau_k^2/\psi_k \geq \gamma_k, \tag{37a}$$

$$\tau_k = \mathbf{h}_k^H\mathbf{w}_k, \quad \psi_k \geq \sigma_c^2 + \sum_{j=1, j\neq k}^{K}\left|\mathbf{h}_k^H\mathbf{w}_j\right|^2, \tag{37b}$$

where (37b) are convex constraints. Then, problem (34) can be reformulated as

$$\max_{\Theta} \quad \omega, \quad \text{s.t.} \quad \omega \leq \frac{\zeta^2}{\phi}, \gamma_k \leq \frac{\tau_k^2}{\psi_k}, \forall k \tag{38a}$$

$$(20b), (34b), (35c), (36), (21a), (22), (37b), \tag{38b}$$

where $\Theta \triangleq \left\{\{\mathbf{W}_k, \mathbf{w}_k\}_{k=1}^K, \omega, t, \phi, \zeta, \tau_k, \psi_k\right\}$ denotes the set of optimization variables. Obviously constraint (38b) is convex. Therefore, the challenge for handling problem (38) lies in the nonconvexity of constraint (38a). To deal with this, we adopt the SCA techniques to establish a convex approximation of constraint (38a). Since function $\frac{\zeta^2}{\phi}$ is jointly convex with respect to ζ and ϕ, its convex lower approximation can be established as

$$\begin{aligned}\frac{\zeta^2}{\phi} &\geq \frac{(\zeta^{(n)})^2}{\phi^{(n)}} + \frac{2\zeta^{(n)}}{\phi^{(n)}}(\zeta - \zeta^{(n)}) - \left(\frac{\zeta^{(n)}}{\phi^{(n)}}\right)^2(\phi - \phi^{(n)}) \\ &= \frac{2\zeta^{(n)}}{\phi^{(n)}}\zeta - \left(\frac{\zeta^{(n)}}{\phi^{(n)}}\right)^2\phi,\end{aligned} \tag{39}$$

where $\zeta^{(n)}$ and $\phi^{(n)}$ are the feasible points obtained at the n-th iteration of the SCA. Consequently, the inner convex approximation of $\omega \leq \frac{\zeta^2}{\phi}$ is

$$\omega \leq \frac{2\zeta^{(n)}}{\phi^{(n)}}\zeta - \left(\frac{\zeta^{(n)}}{\phi^{(n)}}\right)^2\phi. \tag{40}$$

Similarly, the inner convex approximation of $\gamma_k \leq \frac{\tau_k^2}{\psi_k}, \forall k$ is

$$\gamma_k \leq \frac{2\tau_k^{(n)}}{\psi_k^{(n)}}\tau_k - \left(\frac{\tau_k^{(n)}}{\psi_k^{(n)}}\right)^2\psi_k, \forall k, \tag{41}$$

where $\tau_k^{(n)}$ and $\psi_k^{(n)}$ are the feasible points obtained at the n-th iteration.

Finally, a convex approximation of problem (38) is formulated as

$$\max_{\Theta} \quad \omega, \text{ s.t.} \quad (40), (41), (38b). \tag{42}$$

In this way, problem (42) can be solved with off-the-shelf numerical convex program solvers such as CVX Toolbox [43]. We summarize the proposed iterative method in Algorithm 3, where its initial feasible solution can be obtained by following the penalty SCA method given in Remark 2.

Algorithm 3 *: Proposed Iterative Algorithm for Handling* (34)

Initialize $n = 0$, $\Theta^{(0)} \in \mathcal{S}$.
repeat
$n \leftarrow n + 1$;
$\tilde{\mathbf{w}}_k^{(n)} \leftarrow \mathbf{w}_k^{(n-1)}$
Solve problem (42) with $\Theta^{(n-1)}$ and obtain the optimal value $\Theta^{(*)}$;
$\Theta^{(n)} \leftarrow \Theta^{(*)}$;
until Convergence

In the following, we analyze the convergence of Algorithm 3. We can note that in the iterative procedure of Algorithm 3, $\Theta^{(n-1)}$ is always feasible in problem (42) at n-th iteration owing to the adopted first-order Taylor approximation. We note that (42) can be optimally solved and the optimal value of its objective function serves as a lower bound on that of (38). Therefore, it can be guaranteed that the optimal value of (38) at n-th iteration n, denoted as $p_*^{(n)}$, always satisfies $p_*^{(n)} \geq p_*^{(n-1)}$. Therefore, Algorithm 3 produces a non-decreasing objective function of problem (38). Similar to Algorithm 1, the computational complexity of Algorithm 3 is $\mathcal{O}(\sqrt{(2M+1)(K+1)}M^6K^3I_{\text{iter}}\ln(1/\epsilon_0))$.

C. Extended Target Case

For the case of the extended target, following the discussion in Section III-B, we choose $\mathbf{A}$ as the parameter to be estimated and adopt the formulation of CRB in (26). Then, we have the sensing-centric EE for sensing an extended target as

$$\text{EE}_{\text{S}} = \frac{\left(\frac{\sigma_s^2 M}{L}\text{tr}\left(\mathbf{R}_{\mathbf{x}}{}^{-1}\right)\right)^{-1}}{L\left(\frac{1}{\epsilon}\text{tr}(\mathbf{R}_{\mathbf{x}}) + P_0\right)} = \frac{\left(\text{tr}\left(\mathbf{R}_{\mathbf{x}}{}^{-1}\right)\right)^{-1}}{\sigma_s^2 M\left(\frac{1}{\epsilon}\text{tr}(\mathbf{R}_{\mathbf{x}}) + P_0\right)}, \tag{43}$$

where $\mathbf{R_X} = \mathbf{W}\mathbf{W}^H + \tilde{\mathbf{W}}\tilde{\mathbf{W}}^H = \sum_{k=1}^{K} \mathbf{w}_k\mathbf{w}_k^H + \mathbf{R}_{\tilde{\mathbf{W}}}$. Then, we formulate the problem as

$$\max_{\{\mathbf{w}_k\}_{k=1}^K, \mathbf{R}_{\tilde{\mathbf{W}}}} \quad \frac{\left(\mathrm{tr}\left(\mathbf{R_x}^{-1}\right)\right)^{-1}}{\sigma_s^2 M\left(\frac{1}{\epsilon}\mathrm{tr}(\mathbf{R_x}) + P_0\right)} \tag{44a}$$

$$\text{s.t.} \quad \mathrm{tr}(\mathbf{R_x}) \le P_{\max}, \tag{44b}$$

$$\frac{\sigma_s^2 M}{N}\mathrm{tr}\left(\mathbf{R_x}^{-1}\right) \le \phi, \tag{44c}$$

$$\tilde{\mathrm{SINR}}_k \ge \gamma_k, \tag{44d}$$

where $\tilde{\mathrm{SINR}}_k$ is given in (25) and can be recast as a convex form in (30d) by letting $\mathbf{W}_k = \mathbf{w}_k\mathbf{w}_k^H$. We notice that in (44a), the numerator is the reciprocal of a convex function and the denominator is strictly positive and convex. To handle its nonconvexity, we introduce auxiliary optimization variables p_e, q_e and equivalently transform the problem into

$$\max_{\{\mathbf{w}_k\}_{k=1}^K, \mathbf{R}_{\tilde{\mathbf{W}}}, q_e, p_e} \quad \frac{1}{p_e q_e} \tag{45a}$$

$$\text{s.t.} \quad p_e \ge \sigma_s^2 M\left(\frac{1}{\epsilon}\mathrm{tr}(\mathbf{R_x}) + P_0\right), q_e \ge \mathrm{tr}\left(\mathbf{R_x}^{-1}\right), \tag{45b}$$

$$(44\text{b}), (44\text{c}), (44\text{d}). \tag{45c}$$

Then, the problem can be further transformed into its equivalent form as

$$\min_{\{\mathbf{W}_k\}_{k=1}^K, \mathbf{R}_{\tilde{\mathbf{W}}}, q_e, p_e} \quad \ln(p_e) + \ln(q_e) \quad \text{s.t.} \ \ (45\text{b}),\ (45\text{c}), \tag{46}$$

where the objective function is still not convex, but can be approximated based on the first order Taylor series expansion given by

$$\begin{aligned}\ln(p_e) + \ln(q_e) \le & \ln\left(p_e^{(n)}\right) + \ln\left(q_e^{(n)}\right) \\ & + \frac{1}{p_e^{(n)}}\left(p_e - p_e^{(n)}\right) + \frac{1}{q_e^{(n)}}\left(q_e - q_e^{(n)}\right),\end{aligned} \tag{47}$$

where $p_e^{(n)}$ and $q_e^{(n)}$ are the feasible solutions obtained at the n-th iteration. Following the techniques detailed in Section III-B, a convex approximation of problem (45a) at the n-th iteration can be established as

$$\min_{\{\mathbf{W}_k\}_{k=1}^K, \mathbf{R}_{\tilde{\mathbf{W}}}, q_e, p_e} \quad \ln(p_e^{(n)}) + \ln(q_e^{(n)}) \tag{48a}$$

$$+ \frac{1}{p_e^{(n)}}(p_e - p_e^{(n)}) + \frac{1}{q_e^{(n)}}(q_e - q_e^{(n)}) \tag{48b}$$

$$\text{s.t.} \quad (30\text{b}), (30\text{c}), (30\text{d}), (30\text{e}), (45\text{b}). \tag{48c}$$

The computational complexity is $\mathcal{O}(\sqrt{MK + M + K + 1}M^6K^3I_{\mathrm{iter}}\ln(1/\epsilon_0))$ for an ϵ_0-optimal solution.

Theorem 2: Based on the optimal solution of (48a), denoted as $\{\mathbf{W}_k^*, \mathbf{R}_{\tilde{\mathbf{W}}}^*\}$, the optimal rank-1 solutions can always be reconstructed.

Proof: The proof can be achieved by following the proof of Theorem 1 and the details are omitted for brevity. ■

V. Approximate Pareto Boundary of Energy-Efficient ISAC Systems

In this section, we aim to investigate the Pareto boundary of the achievable EE performance region built on the communication-centric EE and the sensing-centric EE. Considering the point-like target case, we follow [44] to formulate the search of the Pareto boundary as a constrained optimization problem that maximizes the communication-centric EE under the sensing-centric EE constraint. It is worth noting that the proposed algorithm can be adapted to the extended target case directly. Now, we aim to solve

$$\max_{\{\mathbf{w}_k\}_{k=1}^K} \frac{\sum_{k=1}^K \log_2\left(1 + \left|\mathbf{h}_k^H\mathbf{w}_k\right|^2 \Big/ \left(\sigma_c^2 + \sum_{j=1, j\ne k}^K \left|\mathbf{h}_k^H\mathbf{w}_j\right|^2\right)\right)}{\frac{1}{\epsilon}\sum_k \|\mathbf{w}_k\|_2^2 + P_0} \tag{49a}$$

$$\text{s.t.} \quad \frac{\mathrm{CRB}^{-1}(\theta)}{L\left(\frac{1}{\epsilon}\sum_{k=1}^K \|\mathbf{w}_k\|_2^2 + P_0\right)} \ge \mathcal{E}, \tag{49b}$$

$$\sum_k \|\mathbf{w}_k\|_2^2 \le P_{\max}, \tag{49c}$$

where $\mathcal{E}$ denotes the required minimum sensing-centric EE threshold. Obviously, problem (49) is a nonconvex fractional program, which is challenging to solve directly. To handle fractional objective function (49a) and nonconvex constraint (49b), we follow [44] to find the approximate optimal Pareto boundary for characterizing the tradeoff between the communication-centric EE and sensing-centric EE.

In particular, we first apply the Dinkelbach algorithm to reformulate fractional function (49a) as

$$\begin{aligned}\max_{\lambda} \ & \sum_{k=1}^K \log_2\left(1 + \frac{\left|\mathbf{h}_k^H\mathbf{w}_k\right|^2}{B_k(\mathbf{W}_k)}\right) - \lambda\left(\frac{1}{\epsilon}\sum_{k=1}^K \mathrm{tr}(\mathbf{W}_k) + P_0\right) \\ \text{s.t.} \ & (21\text{a}),\ (21\text{b}),\end{aligned} \tag{50}$$

where $B_k(\mathbf{W}_k) = \sum_{j=1, j\ne k}^K \mathrm{tr}(\mathbf{Q}_k\mathbf{W}_j) + \sigma_c^2$.

Furthermore, by introducing auxiliary variables b_k, $k = 1, \ldots, K$, the intractable fractional terms in (50) can be equivalently formulated as

$$\begin{aligned}&\sum_{k=1}^K \log_2\left(1 + \frac{\left|\mathbf{h}_k^H\mathbf{w}_k\right|^2}{B_k(\mathbf{W}_k)}\right) \\ &= \max_{b_k}\left(\sum_{k=1}^K \log_2(1+b_k) - \sum_{k=1}^K b_k + \sum_{k=1}^K \frac{(1+b_k)\left|\mathbf{h}_k^H\mathbf{w}_k\right|^2}{B_k(\mathbf{W}_k)}\right),\end{aligned} \tag{51}$$

which has an analytical solution $b_k = \frac{\left|\mathbf{h}_k^H\mathbf{w}_k\right|^2}{B_k(\mathbf{W}_k)}$. Finally, by applying the quadratic transform [32, Theorem 1], problem (49) can be reformulated as (52) at the top on the next page.

The convex approximation of nonconvex constraint (21b) is constraint (22), as mentioned in Section III-A. For handling nonconvex constraint (49b), we introduce an auxiliary variable $\tilde{\mathcal{E}}$ and employ the Schur complement to obtain the convex approximation of problem (49) given by (53) at the top of the next page. (53) is convex whose optimum can be obtained by the interior point method.

$$\max_{\{\mathbf{w}_k\mathbf{W}_k,b_k,t_k\}_{k=1}^K,\lambda} \quad \sum_k \left(\log_2(1+b_k) - b_k + 2t_k\sqrt{(1+b_k)}\,\mathrm{Re}(\mathbf{w}_k^H\mathbf{h}_k) - t_k^2 B_k(\mathbf{W}_k)\right) - \lambda\left(\frac{1}{\epsilon}\sum_{k=1}^K \mathrm{tr}(\mathbf{W}_k) + P_0\right) \tag{52a}$$

$$\text{s.t.} \quad (21a), (21b), (49b), (49c). \tag{52b}$$

$$\max_{\{\mathbf{w}_k\mathbf{W}_k,b_k,t_k\}_{k=1}^K,\lambda} \quad \sum_k \left(\log_2(1+b_k) - b_k + 2t_k\sqrt{(1+b_k)}\,\mathrm{Re}(\mathbf{w}_k^H\mathbf{h}_k) - t_k^2 B_k(\mathbf{W}_k)\right) - \lambda\left(\frac{1}{\epsilon}\sum_{k=1}^K \mathrm{tr}(\mathbf{W}_k) + P_0\right) \tag{53a}$$

$$\text{s.t.} \quad \begin{bmatrix} \mathcal{F}(\sum_{k=1}^K \mathbf{W}_k) - \frac{\tilde{\mathcal{E}}\sigma_s^2}{2L|\alpha|^2} & \sqrt{M}\mathbf{a}^H(\theta)\sum_{k=1}^K \mathbf{W}_k^T\dot{\mathbf{a}}(\theta) \\ \sqrt{M}\dot{\mathbf{a}}^H(\theta)\mathbf{R}_{\mathbf{x}}^T\mathbf{a}(\theta) & \mathbf{a}^H(\theta)\mathbf{R}_{\mathbf{x}}^T\mathbf{a}(\theta) \end{bmatrix} \succeq \mathbf{0}, \tag{53b}$$

$$\tilde{\mathcal{E}} \geq \mathcal{E}N\left(\frac{1}{\epsilon}\sum_{k=1}^K \mathrm{tr}(\mathbf{W}_k) + P_0\right), \tag{53c}$$

$$(21a), (22), (49c). \tag{53d}$$

Therefore, an efficient solution of problem (49) can be obtained by solving a sequence of problem (53). Algorithm 4 summarizes the iterative algorithm, where $\breve{f}_1(\mathbf{w}_k, \mathbf{W}_k) = \frac{\beta}{\overline{\mathcal{R}}}\sum_{k=1}^K\Big(\log_2(1+b_k) - b_k + 2t_k\sqrt{(1+b_k)}\,\mathrm{Re}(\mathbf{w}_k^H\mathbf{h}_k) - t_k^2 B_k(\mathbf{W}_k)\Big) + (1-\beta)\frac{\tilde{\phi}}{L\tilde{\mathcal{C}}}$, $\breve{f}_2(\mathbf{W}_k) = \lambda\left(\frac{1}{\epsilon}\sum_{k=1}^K \mathrm{tr}(\mathbf{W}_k) + P_0\right)$.

Algorithm 4 *: The Proposed Algorithm for Handling Problem* (49)

Initialize $i = 0$, $\delta > 0$, $\{\mathbf{w}_k^{(0)}, \mathbf{W}_k^{(0)}\}_{k=1}^K$ to a feasible value;
repeat
  $i \leftarrow i + 1$;
  $\tilde{\mathbf{w}}_k^{(i)} \leftarrow \mathbf{w}_k^{(i-1)}$
  Update λ by $\lambda^{(i)} = \frac{\breve{f}_1(\mathbf{w}^{(i-1)}, \mathbf{W}^{(i-1)})}{\breve{f}_2(\mathbf{W}^{(i-1)})}$;
  Update b_k by $b_k^{(i)} = \frac{|\mathbf{w}_k^{(i-1)H}\mathbf{h}_k)|^2}{B_k(\mathbf{W}_k^{(i-1)})}$;
  Update t_k by $t_k^{(i)} = \frac{\sqrt{(1+b_k)}\,\mathrm{Re}(\mathbf{w}_k^{(i-1)H}\mathbf{h}_k}{B_k(\mathbf{W}_k^{(i-1)})}$;
  Solve problem (53) to obtain the optimal $\mathbf{w}_k^{(i)}, \mathbf{W}_k^{(i)}$;
until $\breve{f}_1(\mathbf{w}^{(i)}, \mathbf{W}^{(i)}) - \lambda^{(i)}\breve{f}_2(\mathbf{W}^{(i)})$ is less than δ.

VI. Numerical Results

Simulation results of the proposed energy-efficient waveform design are provided in this section. Unless stated otherwise, we consider a dual-functional BS equipped $N = 20$ receiving antennas, with the frame length N set to 30. The maximum transmission power P_{max} is set to 30 dBm with the power amplifier efficiency $\epsilon = 0.35$. The circuit power consumption is set to $P_0 = 30$ dBm. For the target estimation of radar, the target angle is $\theta = 90°$.

A. EE_C Optimization

We first examine the performance of Algorithm 1 for maximizing EE_C considering the existence of a point-like target. The convergence rate of Algorithm 1 is given in Fig. 2a. Obviously, it enjoys a fast convergence rate, whose objective function value converges within 12 iterations on average. Furthermore, the convergence rate of Algorithm 1 is almost the same for different system parameters, e.g., different M and CRB constraints, which confirms the scalability of Algorithm 1.

Fig. 2b investigates the EE_C performance versus the root-CRB threshold for different M. The EE_C increases with the increasing Root-CRB threshold, indicating that EE_C can achieve a higher level when the sensing performance requirement is less stringent. Indeed, increasing the number of antennas can improve EE_C, since more spatial degrees-of-freedom can be utilized for designing an efficient ISAC waveform. Besides, we compare our proposed method with a baseline scheme, which maximizes the achievable communication sum rate under the same constraints of problem (11), including the CRB threshold, SINR requirements, and the power budget, but without regard of the overall EE. Specifically, the sum-rate objective function of the baseline scheme is reformulated into a tractable formulation by using the quadratic-transform as described in Section III-A. The problem is then solved by exploiting the same SDR techniques and linear matrix inequality presented in Section III-A. Obviously, the EE_C of the baseline scheme is unsatisfying, since it only considers the spectral efficiency maximization instead of the EE_C maximization. In such a case, the baseline scheme encourages the ISAC BS to adopt as much power as possible to increase the communication sum rate. Note that while a globally optimal point cannot be guaranteed, our proposed approach still clearly outperforms the state-of-the-art one.

Fig. 2c further demonstrates the EE_C performance versus the circuit power, P_0. It can be seen that increasing P_0 leads to a degradation of EE_C as it also increases the total system power consumption. Besides, compared with the baseline, decreasing P_0 will enlarge the gain obtained by our proposed algorithm. This is because when the circuit power consumption is small, the transmission power constitutes the majority of the overall power consumption, thereby enhancing the relative benefits of our proposed algorithm.

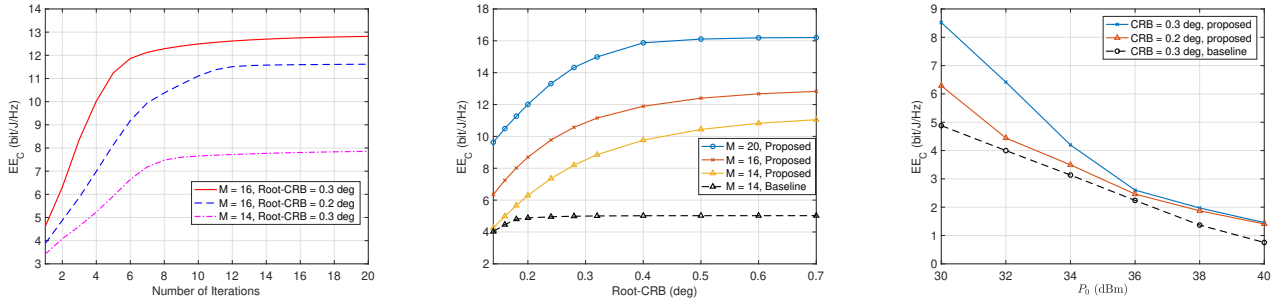

(a) (b) (c)

Fig. 2: (a) $\mathrm{EE_C}$ versus the number of iterations with $\gamma_k = 10$ dB, $K = 3$ for the point-like target case; (b) $\mathrm{EE_C}$ versus different root-CRB thresholds with $\gamma_k = 10$ dB, $K = 2$ for the point-like target case; (c) $\mathrm{EE_C}$ versus different circuit power levels P_0 with $\gamma_k = 10$ dB, $K = 2$, $M = 14$ for the point-like target case.

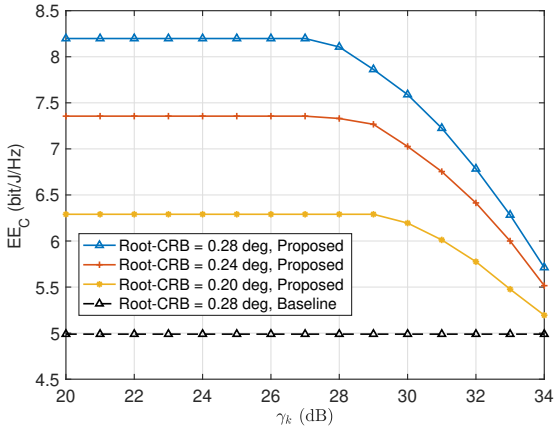

(a)

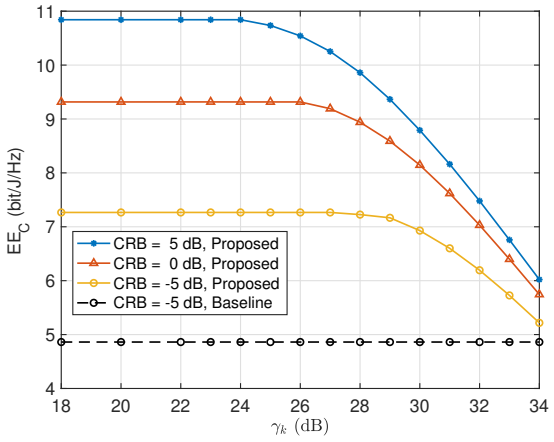

(b)

Fig. 3: $\mathrm{EE_C}$ versus different SINR requirements γ_k. (a) The point-like target case with $M = 14, K = 2$; (b) The extended target case with $M = 14, K = 2$.

Fig. 3a and Fig. 3b plot the $\mathrm{EE_C}$ of the point-like target and extended target with the increasing SINR constraint of multiple users, γ_k, respectively. With the increasing γ_k, $\mathrm{EE_C}$ first remains unchanged and then decreases due to the shrunken feasible region. Therefore, increasing the downlink communication rate does not necessarily improve $\mathrm{EE_C}$. Furthermore, with the increasing root-CRB, the $\mathrm{EE_C}$ decreases, since more power is allocated to radar sensing due to the increasing sensing requirements. A similar trend can also be found in Fig. 3b for the increasing CRB in the extended target case.

B. $\mathrm{EE_S}$ Optimization

In this subsection, we investigate the performance of $\mathrm{EE_S}$ optimization for both the point-like target sensing and extended target cases. In Fig. 4a, we first consider the point-like target to show the $\mathrm{EE_S}$ versus the increasing power budget, for different SINR levels. As expected, $\mathrm{EE_S}$ increases with the increasing P_T, since the increasing power improves the estimation accuracy and increases $\mathrm{EE_S}$. Besides, lowering the SINR requirement also improves $\mathrm{EE_S}$, since relaxing the SINR constraint enlarges the feasible region and improves $\mathrm{EE_S}$. For demonstrating the performance gain obtained by our proposed Algorithm 3, we perform the performance comparison with two other baselines, namely $\mathrm{BA_1}$ and $\mathrm{BA_2}$. In particular, $\mathrm{BA_1}$ aims to minimize the transmission power while $\mathrm{BA_2}$ aims to maximize the communication sum rate under the same constraints as our proposed method (γ_k = 5 dB, the root-CRB threshold is set to 0.15 deg, $P_{\max} = 30$ dBm). The results indicate that $\mathrm{EE_S}$ of $\mathrm{BA_1}$ is significantly low due to the insufficient power for improving the CRB performance. Additionally, $\mathrm{EE_S}$ of $\mathrm{BA_2}$ is also inferior to the proposed method and exhibits a further decline as the transmission power increases, since most of the power is utilized for maximizing the sum rate instead of sensing target.

Fig. 4b further demonstrates the $\mathrm{EE_S}$ versus the SINR requirement, where the root-CRB threshold is set to 0.15 deg. It can be observed that $\mathrm{EE_S}$ decreases as the increasing SINR and the number of communication users since the increasing communication requirements deteriorates the sensing performance. Fig. 4c demonstrates the impact of different circuit power levels, P_0, on the achievable $\mathrm{EE_S}$. As expected,

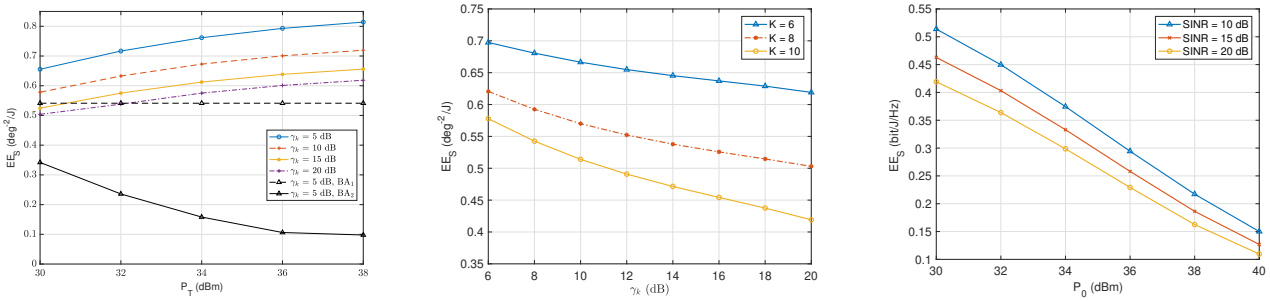

(a) (b) (c)

Fig. 4: (a) $\mathrm{EE_S}$ for the point-like target case versus the maximum transmission power P_T, compared with the baselines, with $M = 16, \rho = 0.15$ deg, $K = 8$. (b) $\mathrm{EE_S}$ for the point-like target case versus the SINR requirements, under different numbers of users, with $M = 16, \rho = 0.15$ deg; (c) $\mathrm{EE_S}$ for the point-like target case versus different circuit power levels P_0, with $K = 10$, $M = 14, \rho = 0.15$ deg.

increasing P_0 will significantly decrease $\mathrm{EE_S}$, indicating that $\mathrm{EE_S}$ can achieve a more satisfactory level with a lower P_0 regardless of the SINR requirements.

As for the scenario of sensing an extended target, Fig. 5a shows the $\mathrm{EE_S}$ versus communication SINR under different numbers of users and different CRB. It is worth noting that the performance metric for the extended target sensing $\mathrm{EE_S}$ is different from the point-like target case. Similar to the scenario of sensing a point-like target, $\mathrm{EE_S}$ decreases with the increasing requirements of communication SINR, especially when the number of users is larger. Besides, increasing CRB requirements improves $\mathrm{EE_S}$, due to the improved estimation performance.

C. Approximate Pareto Boundary of Energy-Efficient ISAC.

Fig. 5b illustrates the approximate Pareto boundary, offering a flexible and scalable tradeoff between $\mathrm{EE_S}$ and $\mathrm{EE_C}$. This tradeoff allows for network designers to switch from $\mathrm{EE_S}$ priority to $\mathrm{EE_C}$ priority and anywhere in between, depending on the specific practical scenario. The inherent conflict between $\mathrm{EE_S}$ and $\mathrm{EE_C}$ also appeals a strategic approach for the designers to strike an effective balance along the Pareto frontier. Besides, from Fig. 5b, we can find that increasing the number of communication users results in a significant deterioration of $\mathrm{EE_S}$, as it consumes more available spatial degrees of freedom, revealing the fact that the tradeoff becomes mode benign with more available degrees of freedom. On the other hand, after the required $\mathrm{EE_S}$ surpasses a certain threshold, there is a sharp decline in $\mathrm{EE_C}$. This is because most of the available resources are allocated for satisfying the stringent $\mathrm{EE_S}$ constraint, leaving insufficient resources for guaranteeing the $\mathrm{EE_C}$ performance. This serves as a reminder that the preset $\mathrm{EE_S}$ value should not surpass a specific threshold, as exceeding this threshold will lead to a significant reduction in $\mathrm{EE_C}$.

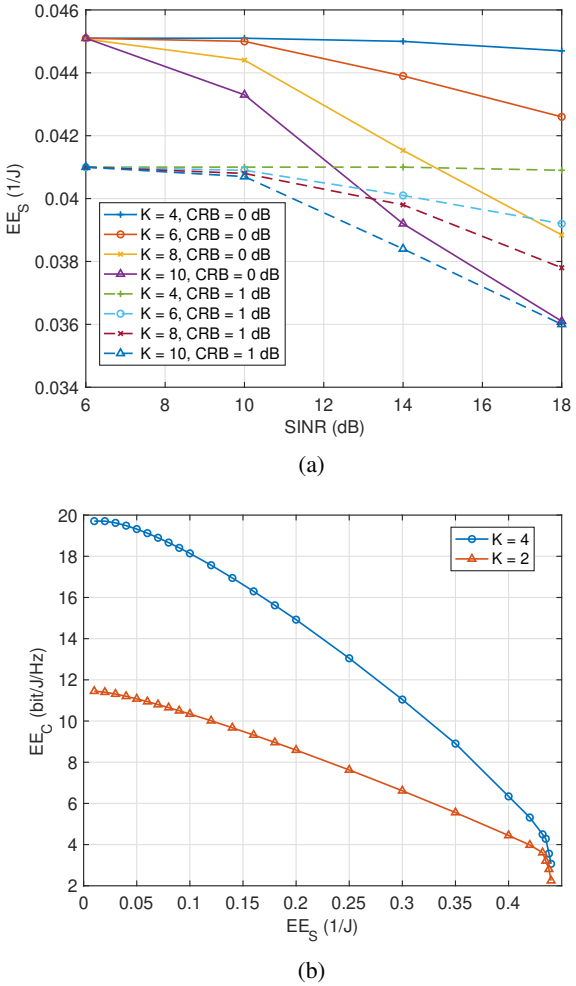

(a)

(b)

Fig. 5: (a) $\mathrm{EE_S}$ in the scenario of sensing an extended target versus the SINR requirement, under different CRB constraints and numbers of users. (b) The Pareto boundary of energy-efficient ISAC for different numbers of communication users with $M = 14$ and $P_{\max} = 30$ dBm.

VII. Conclusion

In this paper, we addressed the problem of maximizing energy efficiency for MIMO ISAC systems. We first studied the communication-centric EE adopting the conventional definition of EE in both the point-like target and extended

$$\mathbf{F}_{\hat{\theta}\hat{\theta}} = \frac{2}{\sigma_s^2}\mathrm{Re}\left[\left(\alpha e^{-j2\pi f_c\tau_c}\mathrm{vec}\left(\dot{\boldsymbol{\Xi}}\mathbf{X}\right)\right)^H\left(\alpha e^{-j2\pi f_c\tau_c}\mathrm{vec}\left(\dot{\boldsymbol{\Xi}}\mathbf{X}\right)\right)\right] = \frac{2|\alpha|^2L}{\sigma_s^2}\mathrm{tr}(\dot{\boldsymbol{\Xi}}\mathbf{R}_{\mathbf{X}}\dot{\boldsymbol{\Xi}}^H), \tag{54a}$$

$$\mathbf{F}_{\hat{\theta}\tau_c} = \frac{2}{\sigma_s^2}\mathrm{Re}\left[\left(\alpha e^{-j2\pi f_c\tau_c}\mathrm{vec}\left(\dot{\boldsymbol{\Xi}}\mathbf{X}\right)\right)^H\left(-j2\pi f_c\alpha e^{-j2\pi f_c\tau_c}\mathrm{vec}\left(\boldsymbol{\Xi}\mathbf{X}\right)\right)\right] = \frac{4\pi f_c|\alpha|^2L}{\sigma_s^2}\mathrm{Re}\left[-j\mathrm{tr}(\boldsymbol{\Xi}\mathbf{R}_{\mathbf{X}}\dot{\boldsymbol{\Xi}}^H)\right], \tag{54b}$$

$$\mathbf{F}_{\tau_c\tau_c} = \frac{2}{\sigma_s^2}\mathrm{Re}\left[\left(-j2\pi f_c\alpha e^{-j2\pi f_c\tau_c}\mathrm{vec}\left(\boldsymbol{\Xi}\mathbf{X}\right)\right)^H\left(-j2\pi f_c\alpha e^{-j2\pi f_c\tau_c}\mathrm{vec}\left(\boldsymbol{\Xi}\mathbf{X}\right)\right)\right] = \frac{-8\pi^2f_c^2|\alpha|^2L}{\sigma_s^2}\mathrm{tr}(\boldsymbol{\Xi}\mathbf{R}_{\mathbf{X}}\boldsymbol{\Xi}^H). \tag{54c}$$

target cases. We reformulated the objective function using the quadratic-transform-Dinkelbach method and solved the sub-problem by leveraging the Schur complement and semi-relaxation techniques. In the second part, we introduced a novel performance metric for measuring sensing-centric EE. We iteratively approximated the objective function as a convex program exploiting SCA to address this problem. Finally, we investigated the tradeoff between the two EE metrics and provided an effective solution. Numerical results showed an improvement compared to the benchmark on both communication-centric EE and sensing-centric EE performance, and we also demonstrated the tradeoff between communication-centric and sensing-centric EE. Future works can consider the energy-efficient ISAC system design for bi-static or multi-static sensing systems.

Appendix A

In this section, we discuss multi-parameter estimation, regarding the time delay and target angle, to achieve location estimation of the target. Considering the time delay, the target response matrix is presented as $\mathbf{H}_r = e^{-j2\pi f_c\tau_c}\mathbf{A} = \alpha e^{-j2\pi f_c\bar{\tau}_c}\mathbf{a}_r(\hat{\theta})\mathbf{a}_t^H(\hat{\theta})$, where τ_c and f_c denote the time delay and the carrier frequency, respectively. Then, the received target echoes can be rewritten as $\tilde{\mathbf{Y}}_{\mathrm{R}} = \mathbf{H}_r\mathbf{X}+\mathbf{Z}_s$. Compared with the sensing model in Section II-B, where only $\hat{\theta}$ is the to-be-estimated parameter, there are two parameters of interest here, i.e., $\hat{\theta}$ and τ_c. To this end, the CRB of $\hat{\theta}$ and τ_c, denoted as $\mathrm{CRB}_{\hat{\theta}}$ and CRB_{τ_c}, respectively, should be both considered in the performance metric and in the optimization problem.

To derive $\mathrm{CRB}_{\hat{\theta}}$ and CRB_{τ_c}, we first vectorize $\tilde{\mathbf{Y}}_{\mathrm{R}}$ as $\tilde{\mathbf{y}}_{\mathrm{R}} = \mathrm{vec}(\tilde{\mathbf{Y}}_{\mathrm{R}}) = \mathrm{vec}(\mathbf{H}_r\mathbf{X})+\tilde{\mathbf{z}}_s = \left(\mathbf{X}^T\otimes\mathbf{I}_N\right)+\tilde{\mathbf{z}}_s$, where $\tilde{\mathbf{z}}_s = \mathrm{vec}(\mathbf{Z}_s)$. Given the observation $\tilde{\mathbf{y}}_{\mathrm{R}}$ that depends on the to-be-estimated parameter $\boldsymbol{\chi} = [\hat{\theta}, \tau_c]^T$, the Fisher information matrix can be given as $[\mathbf{F}]_{ij} = \frac{2}{\sigma_s^2}\mathrm{Re}\left[\frac{\partial\boldsymbol{\mu}^H(\boldsymbol{\chi})}{\partial\boldsymbol{\chi}_i}\cdot\frac{\partial\boldsymbol{\mu}(\boldsymbol{\chi})}{\partial\boldsymbol{\chi}_j}\right]$, where $\boldsymbol{\chi}_i$ and $\boldsymbol{\mu}(\boldsymbol{\chi})$ represent the i-th component of $\boldsymbol{\chi}$ and the mean of $\tilde{\mathbf{y}}_{\mathrm{R}}$ dependent on $\boldsymbol{\chi}_i$, respectively. For brevity, let $\boldsymbol{\Xi} = \mathbf{a}_r(\hat{\theta})\mathbf{a}_t^H(\hat{\theta})$ and $\dot{\boldsymbol{\Xi}} = \frac{\partial\boldsymbol{\Xi}}{\partial\hat{\theta}}$ denoting the partial derivative of $\boldsymbol{\Xi}$ with respect to $\hat{\theta}$. Then, the partial derivations can be calculated as $\frac{\partial\boldsymbol{\mu}(\boldsymbol{\chi})}{\partial\hat{\theta}} = \alpha e^{-j2\pi f_c\tau_c}\mathrm{vec}\left(\dot{\boldsymbol{\Xi}}\mathbf{X}\right)$ and $\frac{\partial\boldsymbol{\mu}(\boldsymbol{\chi})}{\partial\tau} = -j2\pi f_c\alpha e^{-j2\pi f_c\tau_c}\mathrm{vec}\left(\boldsymbol{\Xi}\mathbf{X}\right)$. Then, the elements in $\mathbf{F}$ can be derived as in (54a), (54b), and (54c) at the top of this page, respectively.

Next, following [27], we give the CRB of angel estimation as

$$\mathrm{CRB}_{\hat{\theta}} = \left[\mathbf{F}^{-1}\right]_{11}. \tag{55}$$

Combining (54) and (55), the CRB of angel estimation can be derived as (56) at the top of next page. Similarly, the CRB of time delay estimation can be given as (57) at the top of the next page.

To measure the performance of multiple parameters (location) estimation, we follow [45] and reformulate (33) as

$$\mathrm{EE}_{\mathrm{s}} \triangleq \frac{\frac{\tilde{\rho}_{\hat{\theta}}}{\mathrm{CRB}_{\hat{\theta}}}+\frac{\tilde{\rho}_{\tau_c}}{\mathrm{CRB}_{\tau_c}}}{L\left(\frac{1}{\epsilon}\sum_{k=1}^K\|\mathbf{w}_k\|_2^2+P_0\right)}, \tag{58}$$

where $\tilde{\rho}_{\hat{\theta}}$ and $\tilde{\rho}_{\tau_c}$ are added for unifying the units [45]. It can be noted that (58) shares a nearly identical form as (33). Therefore, our proposed algorithm can be generalized to the case considering the joint estimation of angle and distance, whose details are omitted for brevity.

Appendix B

First, we provide the matrix inequality $\mathbf{W}_k \succeq \mathbf{w}_k\mathbf{w}_k^H$, which satisfies either of the following cases:

Case I: $\mathbf{W}_k \succ \mathbf{w}_k\mathbf{w}_k^H$. Then, we have $\mathrm{tr}(\mathbf{W}_k) > \mathrm{tr}(\mathbf{w}_k\mathbf{w}_k^H)$.

Case II: $\mathbf{W}_k = \mathbf{w}_k\mathbf{w}_k^H$. In this case, we have $\mathrm{tr}(\mathbf{W}_k) = \mathrm{tr}(\mathbf{w}_k\mathbf{w}_k^H)$.

By combining $\mathbf{W}_k \succeq \mathbf{w}_k\mathbf{w}_k^H$ with an additional LMI constraint, given as $\mathrm{tr}(\mathbf{W}_k) \leq \mathrm{tr}(\mathbf{w}_k\mathbf{w}_k^H)$, we can guarantee that Case II always holds. We remark that $\mathrm{tr}(\mathbf{w}_k\mathbf{w}_k^H) = \mathrm{tr}(\mathbf{w}_k^H\mathbf{w}_k) = \mathbf{w}_k^H\mathbf{w}_k$. Further applying the Schur complement, $\mathbf{W}_k = \mathbf{w}_k\mathbf{w}_k^H$ can be equivalently transformed into the following LMI, given as $\begin{bmatrix}\mathbf{W}_k & \mathbf{w}_k\\ \mathbf{w}_k^H & 1\end{bmatrix} \succeq \mathbf{0}, \forall k, \mathrm{tr}(\mathbf{W}_k) - \mathbf{w}_k^H\mathbf{w}_k \leq \mathbf{0}, \forall k$, which completes the proof.

Appendix C

For $K = 1$, we can derive that $\mathbf{h}_k^H\hat{\mathbf{W}}^*\mathbf{h}_k = \mathbf{h}_k^H\mathbf{W}^*\mathbf{h}_k$. Hence, the received SNR and the transmission rate at the user does not decrease. Besides, we have $\mathbf{W}^* - \hat{\mathbf{W}}^* = (\mathbf{W}^*)^{\frac{1}{2}}\left(\mathbf{I}-\frac{(\mathbf{W}^*)^{\frac{1}{2}}\mathbf{h}_k\mathbf{h}_k^H(\mathbf{W}^*)^{\frac{1}{2}}}{\mathbf{h}_k^H\mathbf{W}^*\mathbf{h}_k}\right)(\mathbf{W}^*)^{\frac{1}{2}} \succeq \mathbf{0}$, indicating that the power constraint is satisfied due to $\mathbf{W}^* \succeq \hat{\mathbf{W}}^*$. Additionally, replacing $\mathbf{W}^*$ by $\hat{\mathbf{W}}^*$ would not decrease the transmission rate or increase the total power, showing that $\hat{\mathbf{W}}^*$ is the optimum to the objective function. Then, we discuss the case of $K > 1$. We introduce $r = \mathbf{h}_k^H\left(\mathbf{W}_k+\sum_{i=1,i\neq k}^K\mathbf{W}_i+\mathbf{R}_{\tilde{\mathbf{W}}}+\sigma_C^2\right)\mathbf{h}_k - 1$ and equivalently reformulate (30) as problem (59) shown on the top of the next page.

We note that with the fixed λ, problem (59) is jointly convex of variables $\{\mathbf{W}_k, b_k\}_{k=1}^K, \mathbf{R}_{\tilde{\mathbf{W}}}$. Thus, it can be proved that

$$\mathrm{CRB}_{\hat{\theta}}=\left[\mathbf{F}^{-1}\right]_{11}=\frac{\sigma_s^2\mathrm{tr}(\boldsymbol{\Xi}\mathbf{R}_{\mathbf{X}}\boldsymbol{\Xi}^H)}{2|\alpha|^2L\left(\mathrm{tr}(\dot{\boldsymbol{\Xi}}\mathbf{R}_{\mathbf{X}}\dot{\boldsymbol{\Xi}}^H)\mathrm{tr}(\boldsymbol{\Xi}\mathbf{R}_{\mathbf{X}}\boldsymbol{\Xi}^H)-\mathrm{Re}\left[j\mathrm{tr}(\boldsymbol{\Xi}\mathbf{R}_{\mathbf{X}}\dot{\boldsymbol{\Xi}}^H)\right]\mathrm{Re}\left[j\mathrm{tr}(\boldsymbol{\Xi}\mathbf{R}_{\mathbf{X}}\dot{\boldsymbol{\Xi}}^H)\right]^T\right)}. \tag{56}$$

$$\mathrm{CRB}_{\tau_c}=\frac{\sigma_s^2\mathrm{tr}(\dot{\boldsymbol{\Xi}}\mathbf{R}_{\mathbf{X}}\dot{\boldsymbol{\Xi}}^H)}{2|\alpha|^2L\left(\mathrm{tr}(\dot{\boldsymbol{\Xi}}\mathbf{R}_{\mathbf{X}}\dot{\boldsymbol{\Xi}}^H)\mathrm{tr}(\boldsymbol{\Xi}\mathbf{R}_{\mathbf{X}}\boldsymbol{\Xi})-\mathrm{Re}\left[j\mathrm{tr}(\dot{\boldsymbol{\Xi}}\mathbf{R}_{\mathbf{X}}\boldsymbol{\Xi}^H)\right]\mathrm{Re}\left[j\mathrm{tr}(\dot{\boldsymbol{\Xi}}\mathbf{R}_{\mathbf{X}}\boldsymbol{\Xi}^H)\right]^T\right)}. \tag{57}$$

$$\max_{\{\mathbf{W}_k,b_k\}_{k=1}^K,\mathbf{R}_{\tilde{\mathbf{W}}},\lambda}\sum_{k=1}^K\log(1+r)-\lambda\left(\frac{1}{\epsilon}\mathrm{tr}\left(\sum_{k=1}^K\mathbf{W}_k+\mathbf{R}_{\tilde{\mathbf{W}}}\right)+P_0\right)+\sum_{k=1}^K\left(\log b_k-b_k\left(\sum_{i=1,i\neq k}^K\mathbf{h}_k^H\mathbf{W}_i\mathbf{h}_k+\mathbf{h}_k^H\mathbf{R}_{\tilde{\mathbf{W}}}\mathbf{h}_k+\sigma_C^2\right)\right) \tag{59a}$$

$$\text{s.t. } r=\mathbf{h}_k^H\left(\mathbf{W}_k+\sum_{i=1,i\neq k}^K\mathbf{W}_i+\mathbf{R}_{\tilde{\mathbf{W}}}+\sigma_C^2\right)\mathbf{h}_k-1, \tag{59b}$$

$$\text{(30b), (30c), (30d), (30e), (30f).} \tag{59c}$$

$$\begin{aligned}\mathcal{L}(\mathbf{W}_k)=&-\varpi_{k,1}\mathbf{h}_k^H\mathbf{W}_k\mathbf{h}_k+\sum_{i=1,i\neq k}^K\varpi_{i,1}\mathbf{h}_i^H\mathbf{W}_k\mathbf{h}_i+\varpi_{k,2}\mathbf{h}_k^H\mathbf{W}_k\mathbf{h}_k-\sum_{i=1,i\neq k}^K\varpi_{i,2}\gamma_k\mathbf{h}_i^H\mathbf{W}_k\mathbf{h}_i\\&-\mathrm{tr}(\mathbf{W}_k\boldsymbol{\Psi}_k)+\mu\,\mathrm{tr}(\mathbf{W}_k)+\xi,\end{aligned} \tag{60}$$

Slater's condition holds such that strong duality holds. By introducing the Lagrange multipliers $\varpi_{k,1}\leq 0,\varpi_{k,2}\leq 0,\mu\leq 0$ and $\boldsymbol{\Psi}_k\succeq\mathbf{0}$, we provide the Lagrangian function of $\mathbf{W}_k$ as (60), where ξ represent the terms that do not involve $\mathbf{W}_k$. Then, the KKT conditions of (59) is given as

$$\dot{\mathcal{L}}(\mathbf{W}_k^*)=\mathbf{0},\mathbf{W}_k^*\boldsymbol{\Psi}_k=\mathbf{0}. \tag{61}$$

Then, we have $\boldsymbol{\Psi}_k^*=\mathbf{A}_k^*-\varpi_{k,1}\mathbf{h}_k^H\mathbf{h}_k$ and $\mathbf{A}_k^*=\sum_{i=1,i\neq k}^K\varpi_{i,1}\mathbf{h}_i^H\mathbf{h}_i+\varpi_{k,2}\mathbf{h}_k^H\mathbf{h}_k-\sum_{i=1,i\neq k}^K\varpi_{i,2}\gamma_k\mathbf{h}_i^H\mathbf{h}_i+\mu\mathbf{I}_M$. Nest, we discuss the rank of $\mathbf{A}_k^*$ under the following cases.

1) **Case I**: $\mathrm{rank}(\mathbf{A}_k^*)=M$. In this case, we have $\mathrm{rank}(\boldsymbol{\Psi}_k^*)\geq M-1$ with the inequality $\mathrm{rank}(\mathbf{X}+\mathbf{Y})\geq\mathrm{rank}(\mathbf{X})-\mathrm{rank}(\mathbf{Y})$ [46]. For $\mathrm{rank}(\boldsymbol{\Psi}_k^*)=M$, the first condition in (61) implies $\mathbf{W}_k^*=\mathbf{0}$. For $\mathrm{rank}(\boldsymbol{\Psi}_k^*)=M-1$, we have $\mathrm{rank}(\mathbf{W}_k^*)=1$.

2) **Case II**: $\mathrm{rank}(\mathbf{A}_k^*)=r_a<M$. In this case, we exploit [47, Theorem 2] to construct a rank-1 solution $\mathbf{W}_k^*$. We give $\left\{\mathbf{q}_{k,i}^*\right\}_{i=1}^{M-r_a}$ to denote the columns of orthonormal basis of $\boldsymbol{\Omega}_k^*$, which represents the nullspace of $\mathbf{A}_k^*$. As $\boldsymbol{\Psi}_k^*\succeq\mathbf{0}$, we have $(\mathbf{q}_{k,i}^*)^H\boldsymbol{\Psi}_k^*\mathbf{q}_{k,i}^*=-\varpi_{k,1}|\mathbf{h}_k^H\mathbf{q}_{k,i}^*|^2\geq 0$. Since (59b) should be active at optimum indicating $\varpi_{k,1}\geq 0$, we have $\mathbf{h}_k^H\mathbf{q}_{k,i}^*=0$ and $\boldsymbol{\Psi}_k^*\boldsymbol{\Omega}_k^*=\mathbf{0}$. Thus, the $M-r_a$ dimensions of $\boldsymbol{\Psi}_k^*$'s null space can be represented by $\boldsymbol{\Omega}_k^*$. We further denote $\widetilde{\boldsymbol{\Omega}}_k^*$ as the null-space of $\boldsymbol{\Psi}_k^*$, we have $\mathrm{rank}(\widetilde{\boldsymbol{\Omega}}_k^*)\geq M-r_a$. Additionally, since $\mathrm{rank}(\mathbf{A}_k^*)=r_a$, we have $\mathrm{rank}(\boldsymbol{\Psi}_k^*)\geq r_a-1$, which shows that $\mathrm{rank}(\widetilde{\boldsymbol{\Omega}}_k^*)\leq M-r_a+1$. Then, it can be readily noted that $\mathrm{rank}(\widetilde{\boldsymbol{\Omega}}_k^*)=M-r_a$ or $\mathrm{rank}(\widetilde{\boldsymbol{\Omega}}_k^*)=M-r_a+1$. When $\mathrm{rank}(\widetilde{\boldsymbol{\Omega}}_k^*)=M-r_a$, we have $\mathbf{W}_k^*=\sum_{i=1}^{M-r_a}\lambda_{k,i}^*\mathbf{q}_{k,i}^*(\mathbf{q}_{k,i}^*)^H$ with $\lambda_{k,i}^*\geq 0$. In such a case, $\mathbf{h}_k^H\mathbf{W}_k^*\mathbf{h}_k=0$, which contradicts the optimality. Hence, we conclude that $\mathrm{rank}(\widetilde{\boldsymbol{\Omega}}_k^*)=M-r_a+1$. Denoting $\widetilde{\boldsymbol{\Omega}}_k^*$ as $[\boldsymbol{\Omega}_k^*,\mathbf{p}_k^*]$, the optimal solution $\mathbf{W}_k^*$ can be given as $\mathbf{W}_k^*=\sum_{i=1}^{M-r_a}\lambda_{k,i}^*\mathbf{q}_{k,i}^*(\mathbf{q}_{k,i}^*)^H+\tilde{\lambda}_k^*\mathbf{p}_k^*(\mathbf{p}_k^*)^H$ with $\tilde{\lambda}_k^*\geq 0$. Therefore, a rank-1 solution can be constructed as $\hat{\mathbf{W}}_k^*=\mathbf{W}_k^*-\sum_{i=1}^{M-r_a}\lambda_{k,i}^*\mathbf{q}_{k,i}^*(\mathbf{q}_{k,i}^*)^H=\tilde{\lambda}_k^*\mathbf{p}_k^*(\mathbf{p}_k^*)^H,\hat{\mathbf{R}}_{\tilde{\mathbf{W}}}^*=\mathbf{R}_{\tilde{\mathbf{W}}}^*+\sum_{i=1}^{M-r_a}\lambda_{k,i}^*\mathbf{q}_{k,i}^*(\mathbf{q}_{k,i}^*)^H$.

In the following, we show that the reconstructed solution, $\hat{\mathbf{W}}_k^*$ and $\hat{\mathbf{R}}_{\tilde{\mathbf{W}}}^*$ satisfy the constraints. Firstly, we have $\mathbf{h}_k^H\mathbf{W}_k^*\mathbf{h}_k=\mathbf{h}_k^H\hat{\mathbf{W}}_k^*\mathbf{h}_k,\mathbf{h}_k^H\left(\sum_{i=1,i\neq k}^K\mathbf{W}_i^*+\mathbf{R}_{\tilde{\mathbf{W}}}^*\right)\mathbf{h}_k=\mathbf{h}_k^H\left(\sum_{i=1,i\neq k}^K\hat{\mathbf{W}}_i^*+\hat{\mathbf{R}}_{\tilde{\mathbf{W}}}^*\right)\mathbf{h}_k$. Therefore, the right-hand side term in (59b) and the left-hand side term in (27d) remain unchanged. Besides, it can be readily verified that constraints (27b) and (27c) hold, since $\mathbf{W}_k^*+\mathbf{R}_{\tilde{\mathbf{W}}}^*=\hat{\mathbf{W}}_k^*+\hat{\mathbf{R}}_{\tilde{\mathbf{W}}}^*$, which completes the proof.

REFERENCES

[1] J. Zou, S. Sun, C. Masouros, and Y. Cui, "Sensing-centric energy-efficient waveform design for integrated sensing and communications," in *Proc. IEEE Global Telecommun. Conf. (GLOBECOM)*. Kuala Lumpur, Malaysia, 2023, Accepted.

[2] W. Xu, Z. Yang, D. W. K. Ng, M. Levorato, Y. C. Eldar, and M. Debbah, "Edge learning for B5G networks with distributed signal processing: Semantic communication, edge computing, and wireless sensing," *IEEE*

Journal of Selected Topics in Signal Processing, vol. 17, no. 1, pp. 9–39, Jan. 2023.

[3] A. R. Chiriyath, B. Paul, and D. W. Bliss, "Radar-communications convergence: Coexistence, cooperation, and co-design," *IEEE Trans. Cogn. Commun. Netw.*, vol. 3, no. 1, pp. 1–12, Mar. 2017.

[4] K. Meng, Q. Wu, S. Ma, W. Chen, K. Wang, and J. Li, "Throughput maximization for UAV-enabled integrated periodic sensing and communication," *IEEE Trans. Wireless Commun.*, vol. 22, no. 1, pp. 671–687, Aug. 2022.

[5] J. Zou, R. Liu, C. Wang, Y. Cui, Z. Zou, S. Sun, and K. Adachi, "Aiming in harsh environments: A new framework for flexible and adaptive resource management," *IEEE Network*, vol. 36, no. 4, pp. 70–77, Oct. 2022.

[6] H. Hayvaci and B. Tavli, "Spectrum sharing in radar and wireless communication systems: A review," in *Proc. Int. Conf. IEEE Electromagn. Adv. Appl. (ICEAA)*. Palm Beach, Aruba, Aug. 2014, pp. 810–813.

[7] K.-W. Huang, M. Bică, U. Mitra, and V. Koivunen, "Radar waveform design in spectrum sharing environment: Coexistence and cognition," in *Proc. IEEE Radar Conf. (RadarCon)*. Virginia, USA, May 2015, pp. 1698–1703.

[8] J. A. Zhang, M. L. Rahman, K. Wu, X. Huang, Y. J. Guo, S. Chen, and J. Yuan, "Enabling joint communication and radar sensing in mobile networks—A survey," *IEEE Commun. Surveys Tuts.*, vol. 24, no. 1, pp. 306–345, Oct. 2021.

[9] C. Wang, Z. Li, N. Al-Dhahir, K. J. Kim, and K.-K. Wong, "QoS-Aware precoder optimization for radar sensing and multiuser communications under per-antenna power constraints," *IEEE Trans. Signal Process.*, pp. 1–16, to be published, May 2023.

[10] C. Wang, C.-C. Wang, Z. Li, D. W. K. Ng, K.-K. Wong, N. Al-Dhahir, and D. Niyato, "STAR-RIS-Enabled secure dual-functional radar-communications: Joint waveform and reflective beamforming optimization," *IEEE Trans. Inf. Forensics Secur.*, vol. 18, pp. 4577–4592, Jul. 2023.

[11] R. M. Mealey, "A method for calculating error probabilities in a radar communication system," *IEEE Trans. Space Electron. and Telem.*, vol. 9, no. 2, pp. 37–42, Jun. 1963.

[12] N. David, O. Sendik, H. Messer, and P. Alpert, "Cellular network infrastructure: The future of fog monitoring?" *Bull. Amer. Meteorol. Soc.*, vol. 96, no. 10, pp. 1687–1698, Oct. 2015.

[13] Y. Ma, G. Zhou, and S. Wang, "WiFi sensing with channel state information: A survey," *ACM Comput. Surveys (CSUR)*, vol. 52, no. 3, pp. 1–36, Jun. 2019.

[14] A. Hassanien, M. G. Amin, Y. D. Zhang, and F. Ahmad, "Dual-function radar-communications: Information embedding using sidelobe control and waveform diversity," *IEEE Trans. Signal Process.*, vol. 64, no. 8, pp. 2168–2181, Apr. 2015.

[15] F. Liu, Y.-F. Liu, A. Li, C. Masouros, and Y. C. Eldar, "Cramér-Rao bound optimization for joint radar-communication beamforming," *IEEE Trans. Signal Process.*, vol. 70, pp. 240–253, Dec. 2021.

[16] H. Hua, X. Song, Y. Fang, T. X. Han, and J. Xu, "MIMO integrated sensing and communication with extended target: CRB-rate tradeoff," in *Proc. IEEE Global Telecommun. Conf. (GLOBECOM)*. Rio de Janeiro, Brazil, Jan. 2022, pp. 4075–4080.

[17] Z. Ren, X. Song, Y. Fang, L. Qiu, and J. Xu, "Fundamental CRB-rate tradeoff in multi-antenna multicast channel with ISAC," in *Proc. IEEE Globecom Workshops (GC Wkshps)*. Rio de Janeiro, Brazil, Jan. 2022, pp. 1261–1266.

[18] K. S. V. Prasad, E. Hossain, and V. K. Bhargava, "Energy efficiency in massive MIMO-based 5G networks: Opportunities and challenges," *IEEE Wireless Commun.*, vol. 24, no. 3, pp. 86–94, Jan. 2017.

[19] Y. Wang, C. Li, Y. Huang, D. Wang, T. Ban, and L. Yang, "Energy-efficient optimization for downlink massive MIMO FDD systems with transmit-side channel correlation," *IEEE Trans. Veh. Technol.*, vol. 65, no. 9, pp. 7228–7243, Sep. 2015.

[20] A. Zappone, E. Jorswieck *et al.*, "Energy efficiency in wireless networks via fractional programming theory," *Found. Trends Commun. Inf. Theory*, vol. 11, no. 3-4, pp. 185–396, Jun. 2015.

[21] Z. He, W. Xu, H. Shen, Y. Huang, and H. Xiao, "Energy efficient beamforming optimization for integrated sensing and communication," *IEEE Wireless Commun. Lett.*, vol. 11, no. 7, pp. 1374–1378, Jul 2022.

[22] N. Huang, T. Wang, Y. Wu, Q. Wu, and T. Q. Quek, "Integrated sensing and communication assisted mobile edge computing: An energy-efficient design via intelligent reflecting surface," *IEEE Wireless Commun. Lett.*, vol. 11, no. 10, pp. 2085–2089, Oct. 2022.

[23] J. Xu, L. Qiu, and C. Yu, "Improving energy efficiency through multimode transmission in the downlink MIMO systems," *EURASIP J. Wireless Commun. Netw.*, vol. 2011, no. 1, pp. 1–12, Dec. 2011.

[24] O. Arnold, F. Richter, G. Fettweis, and O. Blume, "Power consumption modeling of different base station types in heterogeneous cellular networks," in *Proc. Future Network Mobile Summit*. Florence, Italy, Mar. 2010, pp. 1–8.

[25] O. Tervo, L.-N. Tran, and M. Juntti, "Optimal energy-efficient transmit beamforming for multi-user MISO downlink," *IEEE Trans. Signal Process.*, vol. 63, no. 20, pp. 5574–5588, Oct. 2015.

[26] C. Jiang and L. J. Cimini, "Energy-efficient transmission for MIMO interference channels," *IEEE Trans. Wireless Commun.*, vol. 12, no. 6, pp. 2988–2999, May 2013.

[27] I. Bekkerman and J. Tabrikian, "Target detection and localization using MIMO radars and sonars," *IEEE Trans. Signal Process.*, vol. 54, no. 10, pp. 3873–3883, Sep. 2006.

[28] J. Li and P. Stoica, "MIMO radar with colocated antennas," *IEEE Signal Process. Mag.*, vol. 24, no. 5, pp. 106–114, Sep. 2007.

[29] R. Schmidt, "Multiple emitter location and signal parameter estimation," *IEEE Trans. Antennas Propag.*, vol. 34, no. 3, pp. 276–280, Mar. 1986.

[30] F. Dong, F. Liu, Y. Cui, W. Wang, K. Han, and Z. Wang, "Sensing as a service in 6g perceptive networks: A unified framework for isac resource allocation," *IEEE Trans. Wireless Commun.*, vol. 22, no. 5, pp. 3522–3536, May 2023.

[31] D. Werner, "On nonlinear fractional programming," *Manage. Sci.*, vol. 13, no. 7, pp. 492–498, Mar. 1967.

[32] K. Shen and W. Yu, "Fractional programming for communication systems—Part I: Power control and beamforming," *IEEE Trans. Signal Process.*, vol. 66, no. 10, pp. 2616–2630, Mar. 2018.

[33] F. Zhang, *The Schur complement and its applications*. Springer Science & Business Media, 2006, vol. 4.

[34] J. Li, C. Bai, Z. Lin, and J. Yu, "Optimized color filter arrays for sparse representation-based demosaicking," *IEEE Trans. Image Process.*, vol. 26, no. 5, pp. 2381–2393, May 2017.

[35] R. G. Ródenas, M. L. López, and D. Verastegui, "Extensions of Dinkelbach's algorithm for solving non-linear fractional programming problems," *Top*, vol. 7, no. 1, p. 33–70, Jun. 1999.

[36] L. You, X. Qiang, K.-X. Li, C. G. Tsinos, W. Wang, X. Gao, and B. Ottersten, "Massive MIMO hybrid precoding for LEO satellite communications with twin-resolution phase shifters and nonlinear power amplifiers," *IEEE Trans. Commun.*, vol. 70, no. 8, pp. 5543–5557, Aug. 2022.

[37] Y. Lu, K. Xiong, P. Fan, Z. Ding, Z. Zhong, and K. B. Letaief, "Global energy efficiency in secure miso swipt systems with non-linear power-splitting eh model," *IEEE J. Sel. Areas Commun.*, vol. 37, no. 1, pp. 216–232, 2019.

[38] A. Ben-Tal and A. Nemirovski, *Lectures on modern convex optimization: Analysis, algorithms, and engineering applications*. SIAM, 2001.

[39] C. Wang, Z. Li, T.-X. Zheng, D. W. K. Ng, and N. Al-Dhahir, "Intelligent reflecting surface-aided secure broadcasting in millimeter wave symbiotic radio networks," *IEEE Trans. Veh. Technol.*, vol. 70, no. 10, pp. 11 050–11 055, Oct. 2021.

[40] Q. Shi, W. Xu, J. Wu, E. Song, and Y. Wang, "Secure beamforming for MIMO broadcasting with wireless information and power transfer," *IEEE Trans. Wireless Commun.*, vol. 14, no. 5, pp. 2841–2853, May 2015.

[41] Y.-H. Li and P.-C. Yeh, "An interpretation of the Moore-Penrose generalized inverse of a singular Fisher Information Matrix," *IEEE Trans. Signal Process.*, vol. 60, no. 10, pp. 5532–5536, Oct. 2012.

[42] P. Pakrooh, A. Pezeshki, L. L. Scharf, D. Cochran, and S. D. Howard, "Analysis of Fisher information and the Cramér–Rao bound for nonlinear parameter estimation after random compression," *IEEE Trans. Signal Process.*, vol. 63, no. 23, pp. 6423–6428, Dec. 2015.

[43] M. Grant and S. Boyd, "CVX: MATLAB software for disciplined convex programming, version 2.1," 2014.

[44] P. Gao, L. Lian, and J. Yu, "Cooperative ISAC with direct localization and rate-splitting multiple access communication: A Pareto optimization framework," *IEEE J. Sel. Areas Commun.*, vol. 41, no. 5, pp. 1496–1515, Jan. 2023.

[45] F. Dong, F. Liu, Y. Cui, W. Wang, K. Han, and Z. Wang, "Sensing as a service in 6G perceptive networks: A unified framework for ISAC resource allocation," *IEEE Trans. Wireless Commun.*, Nov. 2022.

[46] R. A. Horn and C. R. Johnson, *Matrix analysis*. Cambridge university press, 2012.

[47] C. Wang, Z. Li, H. Zhang, D. W. K. Ng, and N. Al-Dhahir, "Achieving covertness and security in broadcast channels with finite blocklength," *IEEE Trans. Wireless Commun.*, vol. 21, no. 9, pp. 7624–7640, Mar. 2022.